UC Irvine
UC Irvine Previously Published Works

Title

Parasite inversion for determining the coefficients and time-validity of Philip's two-term infiltration equation

Permalink

Journal

ISSN

Authors

Jaiswal, Parakh
Gao, Yifu
Rahmati, Mehdi
et al.

Publication Date

DOI

Peer reviewed

ORIGINAL RESEARCH ARTICLE

Vadose Zone Journal OPEN ACCESS

Parasite inversion for determining the coefficients and time-validity of Philip's two-term infiltration equation

Parakh Jaiswal[1] | **Yifu Gao[1]** | **Mehdi Rahmati[2,3]** | **Jan Vanderborght[3]** | **Jirka Šimůnek[4]** | **Harry Vereecken[3]** | **Jasper A. Vrugt[1,5]**

[1] Dep. of Civil and Environmental Engineering, Univ. of California, Irvine, CA 92697, USA

[2] Dep. of Soil Science and Engineering, Faculty of Agriculture, Univ. of Maragheh, Maragheh, Iran

[3] Forschungszentrum Jülich, Institute of Bio- and Geosciences: Agrosphere (IBG-3), Jülich, Germany

[4] Dep. of Environmental Sciences, Univ. of California, Riverside, CA 92521, USA

[5] Dep. of Earth System Science, Univ. of California, Irvine, CA 92697, USA

Correspondence
Harry Vereecken, Forschungszentrum Jülich, Institute of Bio- and Geosciences: Agrosphere (IBG-3), Jülich, Germany.
Email: h.vereecken@fz-juelich.de

Assigned to Associate Editor Nima Shokri.

Abstract

Many different equations have been proposed to describe quantitatively one-dimensional soil water infiltration. The unknown coefficients of these equations characterize soil hydraulic properties and may be estimated from a n record, $\{\tilde{t}_i, \tilde{I}_i\}_{i=1}^{n}$, of cumulative infiltration measurements using curve fitting techniques. The two-term infiltration equation, $I(t) = S\sqrt{t} + cK_s t$, of Philip has been widely used to describe measured infiltration data. This function enjoys a solid mathematical–physical underpinning and admits a closed-form solution for the soil sorptivity, S [L T$^{-1/2}$], and multiple, c [−], of the saturated hydraulic conductivity, K_s [L T^{-1}]. However, Philip's two-term equation has a limited time validity, t_{valid} [T], and thus cumulative infiltration data, $\tilde{I}(\tilde{t})$, beyond $t = t_{valid}$ will corrupt the estimates of S and K_s. This paper introduces a novel method for estimating S, c, K_s, and t_{valid} of Philip's two-term infiltration equation. This method, coined parasite inversion, use as vehicle Parlange's three-parameter infiltration equation. As prerequisite to our method, we present as secondary contribution an exact, robust and efficient numerical solution of Parlange's infiltration equation. This solution admits Bayesian parameter estimation with the DiffeRential Evolution Adaptive Metropolis (DREAM) algorithm and yields as byproduct the marginal distribution of Parlange's β parameter. We evaluate our method for 12 USDA soil types using synthetic infiltration data simulated with HYDRUS-1D. An excellent match is observed between the inferred values of S and K_s and their "true" values known beforehand. Furthermore, our estimates of c and t_{valid} correlate well with soil texture, corroborate linearity of the $c(\beta)$ relationship for $0 \leq t \leq t_{valid}$, and fall within reported ranges. A cumulative vertical infiltration of about 2.5 cm may serve as guideline for the time-validity of Philip's two-term infiltration equation.

1 | INTRODUCTION AND SCOPE

The topic of water infiltration into unsaturated soils has attracted the attention of vadose zone hydrologists early on. This process lends itself for detailed experimentation, mathematical–physical analysis, and spatiotemporal modeling and is central to hydrologic studies by water resource and hydraulic engineers, hydrogeophysicists, hydrogeologists, plant scientists, agronomists, and ecologists (Philip, 1969b). Infiltration not only determines how much rainfall (irrigation) will accumulate on the soil's surface or runoff elsewhere following topographical gradients, but it also exerts control on the soil moisture status of the root zone, which, in turn, regulates processes such as the absorption of soil water by plant roots, evaporation, sensible heat fluxes, and groundwater recharge (Liu et al., 2011). Infiltration will also govern the transport of pollutants through the vadose zone, slope stability, and land subsidence in areas that rely heavily on groundwater pumping as primary water source (Chen et al., 2014). Farmers in the Central Valley of California, for example, rely heavily on infiltration to maintain an adequate soil moisture status of the root zone in pursuit of an optimal crop yield (Hellin & Schrader, 2003; Schoups et al., 2005).

After the topsoil has absorbed sufficient rainfall (or irrigation water), the water moves downward in the soil profile under the influence of gravity and/or capillary action, soaking and/or filling up the pore space, replenishing the root zone, and possibly seeping into rocks through cracks. Infiltrability is a term native to soil physics and hydrology that defines the maximum rate at which rain or irrigation water can be absorbed by a soil under given conditions (Horton, 1933). The infiltration rate under natural conditions is not necessarily readily deducible from soil moisture measurements, certainly at larger spatial scales, and infiltration modeling with the aid of measurable quantities is of fundamental importance.

In the past decades, numerous mathematical–physical approaches have been developed to describe water infiltration into the vadose zone (Assouline, 2013). These models or functions can be classified as empirical, semiempirical and (quasi-) mechanistic. Empirical infiltration models are mathematical functions that have been crafted by trial and error with the sole purpose of matching laboratory or field measured cumulative infiltration, $I(t)$ [L], data, where t [T] denotes time. The resulting black-box function offers no insights into the underlying data-generating process nor provides evidence why the function would accurately portray the n vector of measured cumulative infiltration data. Examples include the infiltration equations of Kostiakov (1932), Huggins and Monke (1966), modified Kostiakov (Smith, 1972), and Collis-George (1977). As the parameters of empirical infiltration models lack a theoretical foundation, it is typically difficult, if not impossible, to relate their fitted values to physical soil properties. Semiempirical (gray-box) infiltra-

Core Ideas

- We describe a method that can determine the time validity of infiltration equations.
- This method infers as well the hydraulic properties of unsaturated soils.
- We present a robust and efficient numerical solution of Parlange's three-parameter infiltration equation.
- Posterior distribution determines how well parameters are defined by calibration to data.
- Two and a half centimeters of cumulative infiltration is a good proxy for time validity Philip's two-term equation.

tion models conserve mass with a flux–concentration (storage) relationship that relates the infiltration rate, i [L T^{-1}], to the cumulative infiltration, I, which is usually hypothesized. Examples include the models of Horton (1941), Holtan (1961), Singh and Yu (1990), and Grigorjev and Iritz (1991). Then, the last group of quasi-deterministic (white-box) infiltration models adopt a reductionist approach and describe the downward and/or horizontal movement of water using mass balance principles coupled with a macroscopic law for soil moisture flow. This use of first principles offers a robust protection against invalid assumptions and conventions and includes the mechanistic models of Green and Ampt (1911), Philip (1957, 1969a), Mein and Larson (1971, 1973), Smith (1972), Braester (1973), Stroosnijder (1976), Brutsaert (1977), Smith and Parlange (1978), Haverkamp et al. (1994), Salvucci and Entekhabi (1994), Basha (1999, 2000, 2002), Zhu and Mohanty (2002), Chen and Gallipoli (2004), and Valiantzas (2010). These models vary in complexity and degree of sophistication and differ in their assumptions about infiltration source type (point, circular, strip, and rectangular) and location (above- or belowground), the shape of the infiltration front, soil heterogeneity, dominant processes and flow dynamics, the hydraulic functions, and initial and boundary conditions.

The mathematical–physical description of the infiltration process has benefited tremendously from the theories and heavy lifting of Dr. John Philip (1927–1999). While he has been recognized internationally for his many contributions to the topics of water, gas, and energy movement, his research on infiltration is arguably the most acclaimed worldwide. Dr. Philip's advanced mathematical training and deep intuition about physical processes enabled him to make fundamental advances to the theory and practice of water infiltration. In a classic treatise on one-dimensional infiltration, Philip (1957) describes the cumulative vertical infiltration, $I(t)$, as a finite

(convergent) series of $d > 3$ expansion terms:

$$
\begin{aligned}
I(t) &= a_1 t^{\frac{1}{2}} + a_2 t + a_3 t^{\frac{3}{2}} + \cdots + a_d t^{\frac{d}{2}} \\
&= \sum_{j=1}^{d} a_j t^{\frac{j}{2}},
\end{aligned}
\tag{1}
$$

where a_1 [L T$^{-1/2}$], a_2[L T^{-1}], a_3 [L T$^{-3/2}$], and a_d [L T$^{-d/2}$] are soil-dependent constants, and t denotes time. Philip (1957) showed that a_1 is synonymous to the sorptivity, S [L T$^{-1/2}$], a measure of the soil's capacity to take up and release liquids by capillarity, and a_2 is equal to a multiple, c, of the saturated hydraulic conductivity, K_s [L T^{-1}], which articulates a soil's ability to transmit water under the influence of gravity. Philip (1969a) expressed the soil sorptivity as follows

$$
S(\theta_i) = \int_{\theta_i}^{\theta_s} \lambda(\theta) d\theta
\tag{2}
$$

where θ_i [L^3 L^{-3}] denotes the initial water content of the soil (assumed uniform), θ_s [L^3 L^{-3}] is the volumetric moisture content at saturation, and $\lambda(\theta)$ [L T$^{-1/2}$] is the so-called Boltzmann variable:

$$
\lambda(\theta) = z(\theta, t) t^{-1/2}
\tag{3}
$$

The characteristic function, $z(\theta, t)$, expresses the relationship between soil depth, z [L], and the volumetric water content, θ [L^3 L^{-3}], at time $t \geq 0$ during an infiltration event under gravity-free conditions, where $\theta_i \leq \theta \leq \theta_s$. For notational convenience, we omit the explicit functional dependence of the soil sorptivity, S, on the initial moisture content. Thus, the first two coefficients, a_1 and a_2, of Philip's time series expansion exhibit a sound physical underpinning, adjustable to the initial and boundary conditions of the infiltration event.

The finite series of expansion terms of Philip (1957) not only benefits a solid theoretical underpinning but also enjoys a more practical advantage. As the cumulative infiltration, $I(t)$, is written as a multiple of the coefficients, a_j ($j = 1, \ldots, d$), of the d expansion terms, Equation 1 admits the application of linear regression to determine the optimum parameter values and their associated uncertainty from a dataset, $\{\tilde{t}_i, \tilde{I}_i\}_{i=1}^{n}$, of n cumulative infiltration measurements, $\tilde{I}_1, \tilde{I}_2, \ldots, \tilde{I}_n$, observed at $\tilde{t}_1, \tilde{t}_2, \ldots, \tilde{t}_n$. Indeed, as Equation 1 belongs to the class of linear regression models, we can write Philip's infiltration function as an inner product, $I(t) = \mathbf{d}(t)^\top \mathbf{a}$, of a $d \times 1$ design vector, $\mathbf{d}(t) = [t^{1/2} \ \ t \ \ t^{3/2} \ \cdots \ t^{d/2}]^\top$, and the d vector, $\mathbf{a} = [a_1 \ \ a_2 \ \ a_3 \ \cdots \ a_d]^\top$, of parameters. If we stack the design vectors, $\mathbf{d}(\tilde{t})$ of the n measurement times, $\tilde{t}_1, \tilde{t}_2, \ldots, \tilde{t}_n$, in a $n \times d$ design matrix, $\mathbf{D}$, then the least squares parameter values, $\hat{\mathbf{a}} = [\hat{a}_1 \ \ \hat{a}_2 \ \ \hat{a}_3 \ \cdots \ \hat{a}_d]^\top$, of the measured cumulative infiltration data, $\tilde{\mathbf{I}} = [\tilde{I}_1 \ \ \tilde{I}_2 \ldots \tilde{I}_n]^\top$, will equal, $\hat{\mathbf{a}} = (\mathbf{D}^\top \mathbf{D})^{-1} \mathbf{D}^\top \tilde{\mathbf{I}}$.

Philip (1957) postulated that coefficients $a_3, a_4, \ldots, a_d$, of Equation 1 must satisfy the following constraint:

$$
\frac{a_j}{S} > \left(\frac{a_2}{S}\right)^{j-1}
\tag{4}
$$

for all $j = (3, \ldots, d)$. This constraint implies that all coefficients $a_3, a_4, \ldots, a_d$ must exceed zero, and, as a result, Equation 1 will not converge to a constant infiltration rate at large t. Instead, Equation 4 promotes significance of the higher order terms at the potential risk of overfitting (Volpi et al., 2017). This is also known as Runge's phenomenon (polynomial wiggle) and cautions against the use of a large number of expansion terms. The most popular variant of Equation 1 uses only two expansion terms:

$$
I(t) = S t^{1/2} + c K_s t
\tag{5}
$$

where the multiplicative coefficient c is soil dependent. This two-term formulation enjoys a rigorous mathematical–physical underpinning. This includes recent work of Hunt et al. (2017), who used percolation theory to interpret S and $c K_s$. The use of $d = 2$ expansion terms, however, has an important side effect. As the higher order expansion terms of Equation 1 are discarded, Philip's two-term equation cannot describe adequately the infiltration at later times when the higher order terms have an increasingly larger impact on the cumulative infiltration. In other words, Philip's two-term equation has a limited time validity, t_{valid} [T] and, consequently, cumulative infiltration measurements beyond t_{valid} should not be used for parameter estimation purposes, as these measurements will corrupt estimates of the soil sorptivity, S, and saturated hydraulic conductivity, K_s.

In his theoretic treatise, Philip (1957) derived a simple analytic expression for the so-called characteristic time, t_{char} [T], of Equation 1:

$$
t_{char} = \left(\frac{S}{K_s - K_i}\right)^2
\tag{6}
$$

at which gravity and capillary action contribute equally to the instantaneous infiltration. In this equation, $K_i = K(\theta_i)$ [L T^{-1}] is the soil hydraulic conductivity at the initial moisture content. Philip (1957) used the characteristic time, t_{char}, to demarcate the window for which Equation 1 is valid. Specifically, he postulated that the finite series of $d \geq 3$ expansion terms is valid only for infiltration times up to $2t_{char}$ to $4t_{char}$. We should be careful, however, in using these estimates for Philip's two-term infiltration (Equation 5). Without doubt, the truncation of (1) to $d = 2$ terms must deteriorate the time validity of the two-term formulation. Indeed, practical guidelines are warranted on the time validity, t_{valid}, of Equation 5.

In this paper, we introduce a new method for determining the values of the dimensionless coefficient c, soil properties S and K_s, and time validity t_{valid} of Philip's two-term infiltration equation. We cannot infer these four quantities simultaneously from measured cumulative infiltration curves as this constitutes an ill-posed problem. Therefore, we divide the inference in two separate steps using an approach coined parasite inversion. The first step takes advantage of the infiltration equation of Parlange et al. (1982), an quasi-exact solution of Richards' equation to back out the values of S and K_s from a collection of measured $(\tilde{t}, \tilde{I})$ data pairs using Bayesian inference with the DREAM$_{(ZS)}$ algorithm with sampling from past states (Vrugt, 2016). To this end, we present a robust, efficient, and exact numerical solution of Parlange's infiltration equation, which generalizes existing solutions of Latorre et al. (2015) and Fernández-Gálveza et al. (2019) to warrant treatment and estimation of all its four parameters: S, K_s, K_i, and β. In a second step, the maximum a posteriori density values of S and K_s are admitted to Philip's two-term infiltration equation to yield estimates of c and t_{valid}. We benchmark, test, and evaluate our approach using synthetic infiltration data simulated by HYDRUS-1D (Šimůnek et al., 2008). Our approach has some elements in common with Dohnal et al. (2010), who used the infiltration equation of Haverkamp et al. (1994) with $\beta = 0.6$ to estimate S and K_s from synthetic infiltration data of a three-dimensional axisymmetric soil model. The optimized values of S and K_s were entered in Philip's two-term Equation 5 to simulate one-dimensional infiltration.

The remainder of the paper is organized as follows. Section 2 introduces the cumulative infiltration data that is used to test, benchmark, and evaluate our two-step procedure. In Section 3, we detail the different building blocks of our methodology. This is followed in Section 4 with a presentation and discussion of our results. In Section 5, we briefly discuss the main implications of this paper and present a simplified implementation of our methodology. Finally, Section 6 concludes this paper with a summary of the main findings.

2 | SYNTHETIC INFILTRATION DATA

To benchmark, test, and evaluate our method, we are in need of cumulative infiltration data and corresponding estimates of the soil sorptivity, S, and the saturated hydraulic conductivity, K_s. These two soil properties should be known beforehand, otherwise we cannot verify that our estimates of S and K_s are unbiased and accurate. Practical experience suggests that it is not particularly easy to accurately determine the soil sorptivity. This necessitates infiltration measurements under gravity-free conditions when water flow is largely controlled by capillary adsorption or desorption. This requires considerable experimental effort, particularly if we wish to evaluate our method for many different soil types. What is more, our

analysis demands a high temporal measurement resolution to accurately pinpoint the time validity of Philip's two-term infiltration equation. Therefore, we resort to synthetic infiltration data in this paper, as this allows control on data quality and quantity. We did evaluate our method for measured data as well using the more than 1,300 infiltration experiments documented in the Soil Water Infiltration Global (SWIG) database (Rahmati, Weihermüller, Vanderborght, et al., 2018; Rahmati, Weihermüller, & Vereecken, 2018). Only a small number of these experiments have a data quality and quantity sufficient enough to warrant application of our methodology. These results (not shown here) corroborate our findings for the synthetic infiltration data.

Vertical infiltration into a 200-cm-deep homogeneous soil was simulated with HYDRUS-1D (Šimůnek et al., 2008, 2016) using the hydraulic functions of Mualem–van Genuchten (MVG) (Mualem, 1976; van Genuchten, 1980). The soil is initialized as dry by setting the hydraulic head of the column equal to −15,000 cm (except for sand, we used −1,000 cm). Cumulative infiltration is then simulated for a period of 240 h using a constant pressure head at the surface and free drainage condition at the bottom of the soil profile (see also Rahmati et al., 2020). Table 1 lists the MVG parameter values of the HYDRUS-1D catalog that were used to simulate the infiltration data for each soil type.

As soil column discretization may affect the numerical results, we used HYDRUS-1D to simulate horizontal infiltration for an ensemble of discretized profiles. The simulated infiltration was compared against an analytic solution for infiltration without gravity, which is based on the Boltzmann transform. For each discretized profile, the simulated water content distribution in the soil column was plotted against the Boltzmann variable, λ, in Equation 2. A discretized profile is deemed accurate if the (θ, λ) relationships at many different simulation times coalesce in one single curve. The highest simulation accuracy was achieved with a profile composed of 401 nodes using an entrance node of 10^{-6} cm and gradually increasing size of the elements in the profile up to 1 cm for the last node. This profile was subsequently used to simulate vertical infiltration. To negate numerical errors and promote accuracy of the simulated vertical infiltration, the internal interpolation tables of (θ, h) and (h, K) were disabled, and the default initial time step of HYDRUS-1D was adjusted to satisfy convergence criteria for all different USDA soils. What is more, a modified MVG model with air-entry value of −2 cm was used for soils with $n_{VG} < 1.2$ to avoid unrealistically large changes in the hydraulic conductivity near saturation (Schaap & van Genuchten, 2006; Vogel & Cislerova, 1988; Vogel et al., 2000).

Before we can analyze the vertical infiltration experiments of HYDRUS-1D, we must first post-process the simulated output (between 1,200 and 13,000 print times) so as to yield a common data length and format for each soil. First, we

TABLE 1 Values of the van Genuchten (1980) soil hydraulic parameters for the 12 USDA textural classes derived from Carsel and Parrish (1988)

Parameters	θ_i	θ_s	θ_r	α	n_{VG}	$\tilde{S}$	$\tilde{K}_s$
		cm³ cm⁻³		cm⁻¹		cm h⁻¹/²	cm h⁻¹
Clay	0.271	0.380	0.068	0.008	1.09	1.02	0.200
Clay loam	0.150	0.410	0.095	0.019	1.1	1.45	0.260
Loam	0.088	0.430	0.078	0.036	1.56	2.19	1.040
Loamy sand	0.057	0.410	0.057	0.124	2.28	6.20	14.59
Sand	0.045	0.430	0.045	0.145	2.68	9.21	29.70
Sandy clay	0.170	0.380	0.100	0.027	1.23	0.78	0.120
Sandy clay loam	0.111	0.390	0.100	0.059	1.48	1.60	1.310
Sandy loam	0.066	0.410	0.065	0.075	1.89	3.3	4.421
Silt	0.090	0.460	0.034	0.016	1.37	1.34	0.250
Silt loam	0.104	0.450	0.067	0.020	1.41	1.65	0.450
Silt clay	0.266	0.360	0.070	0.005	1.09	0.35	0.020
Silty clay loam	0.197	0.430	0.089	0.010	1.23	0.52	0.070

Note. The last two columns list the saturated soil hydraulic conductivity, $\tilde{K}_s$, and sorptivity, $\tilde{S}$, which are of main interest in the present study. The tilde operator is used for both variables to signify "measured" quantities. The soil sorptivity, $\tilde{S}$, is computed with Equation 2 using HYDRUS-1D simulated moisture profiles of a horizontal infiltration experiment with initial water content, θ_i, θ_s, saturated water content; θ_r, residual water content; α and n_{VG}, van Genuchten parameters.
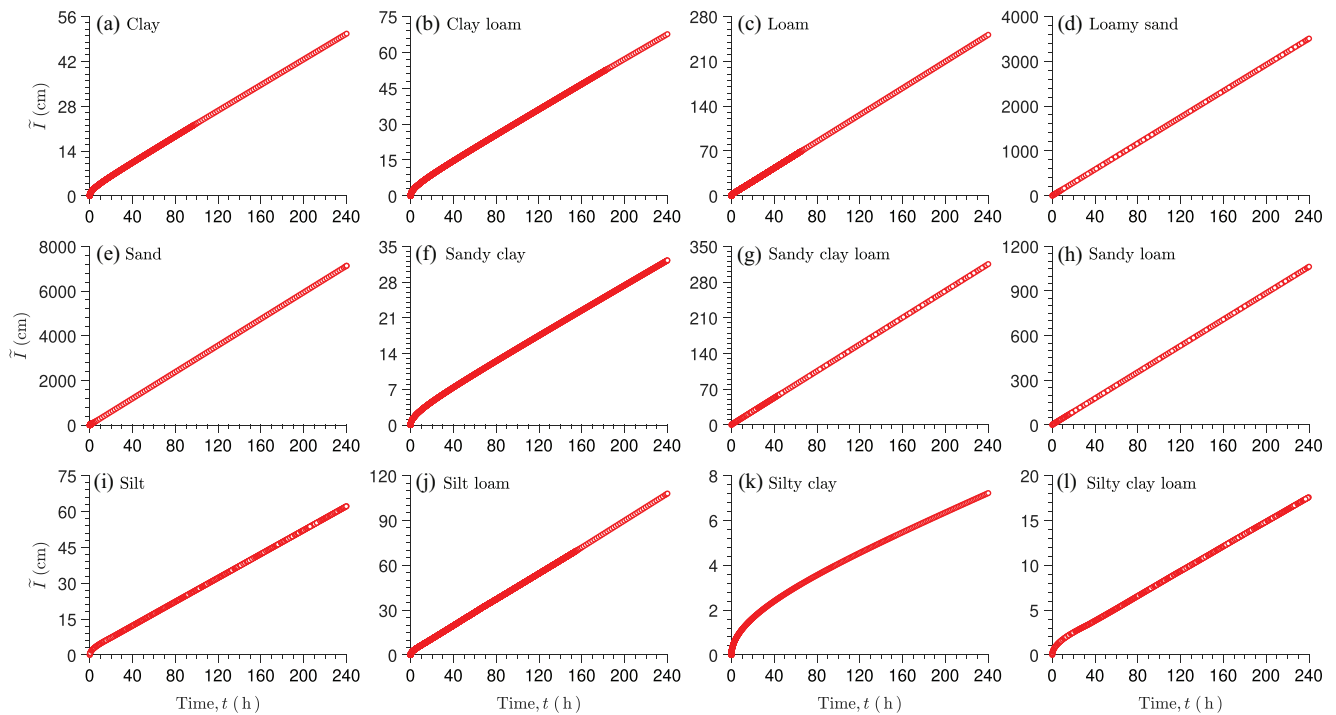
FIGURE 1 HYDRUS-1D simulated cumulative infiltration, $\tilde{I}$, data for a 200-cm homogeneous soil profile using the Mualem–van Genuchten (MVG) hydraulic functions with parameter values of the 12 different textural classes documented in Table 1. A constant pressure head was assumed at the soil surface, and a free drainage condition was imposed at the bottom boundary of the profile. The HYDRUS-1D output is post-processed to limit the cumulative infiltration for each soil type to 5 cm

synchronize the print times of the datasets. To this end, we discretize the 240-h simulation period into $n = 100$ equally spaced print times on a logarithmic (base 10) scale. The cumulative infiltration at each print time (query point) is then computed from the raw HYDRUS-1D output using linear interpolation. Logarithmic scaling of the print times guarantees a high measurement resolution at the beginning of the infiltration experiment. This is deemed necessary to portray accurately the relatively high infiltration rates early on in the experiment. Figure 1 presents the post-processed infiltration curves of each USDA soil type using 100 logarithmically scaled measurement times. The simulation period of 240 h is too large to notice subtle differences in the functional shape of the infiltration curves at early times. Nevertheless, it is evident that the soils differ substantially in the amount of cumulative infiltration. For example, sand (Figure 1E) has infiltrated more than 7,000 cm of water, whereas the clay soil (Figure 1A) barely reaches 50 cm in the same time period of 240 h. In theory, one would expect clay to infiltrate the least amount of water. However, the sandy clay (Figure 1F), silty clay (Figure 1L), and silty clay loam (Figure 1L) soils infiltrate only 32.2, 7.2, and 17.6 cm of water, respectively, over the 240-h period. To understand this finding, we must look at the hydraulic properties of the different soils. According to Table 1, the sandy clay, silty clay, and silty clay loam soils exhibit the lowest sorptivity, S, and saturated hydraulic conductivity, K_s, of all 12 soils.

Thus, the MVG parameter values, as documented in Carsel and Parrish (1988) and used in the HYDRUS-1D catalog, may not portray accurately the hydraulic properties of each textural class. It should suffice to say that the post-processed infiltration curves are a nearly perfect match with the raw output of HYDRUS-1D. Their distance is negligible small.

A last comment about the numerical accuracy of the simulated infiltration data is in order. Our experience suggests, that it is not always easy to simulate accurately infiltration experiments. For example, a careful examination of the simulated data of silty clay loam demonstrates a minor dip in the cumulative infiltration at $t = 30$ h. This artifact is small and may not catch everyone's attention; nevertheless, the subtle, unexpected variations in the infiltration rate may explain in part why silty clay loam is classified as one of our two dissonant soils. As we have devoted special care and attention to numerical errors, we are confident that the current dataset is robust and accurate for all soils, with possible exception of sandy clay loam and silty clay loam.

The logarithmically scaled infiltration curves use synchronized measurement times yet correspond to an infiltration event of 240 h. For most soils, this duration is excessive and far exceeds the time at which a constant infiltration rate is reached. What is more, in field experiments, the cumulative infiltration is typically limited, as the soil underneath may not be homogeneous over a very large depth. Hence, we should

adjust the duration of the experiment so as to have a reasonable amount of infiltration for each soil type. For example, if we assume a porosity $\phi = 0.4$ and initial moisture content $\theta_i = 0.1$, then about 3 cm of cumulative infiltration would suffice to bring the top 10 cm of the soil to saturation. Continued infiltration is not expected to yield more information about the topsoil's hydraulic properties.

For reasons detailed above, we do not proceed with this first dataset but create a second dataset from the raw output of HYDRUS-1D wherein we limit the cumulative infiltration to 5 cm. In doing so, we divide the raw output of HYDRUS-1D into equally spaced intervals of 0.05 cm. This results in $n = 100$ measurements of the cumulative infiltration. The corresponding measurement times are derived via linear interpolation using the raw HYDRUS-1D output. Thus, the measurement times in this second dataset correspond to cumulative infiltration values of 0.05, 0.10, 0.15, ..., 5.00 cm. The so-obtained measurement times differ substantially among the different soil types. Sand, for instance, only needs a handful of minutes to infiltrate 5 cm of water, whereas the silty clay soil requires about 150 h to do so. This second dataset is used throughout the remainder of this paper. In anticipation of experimental data, we refer to this second dataset as *measured data* or *measured infiltration data*. This fixes the notation.

Now we have discussed the vertical infiltration data simulated with HYDRUS-1D, we are left with estimation of the "true" sorptivity, S, for each soil type. Unlike the saturated hydraulic conductivity, K_s, the sorptivity, S, is not invariant but dependent on the soil's initial moisture content. Hence, S is not an innate property of the MVG model but a by-product of the hydraulic parameters, θ_s, θ_r, α, n_{VG}, and K_s listed in Table 1 and the uniform initial moisture content, θ_i, of the 200-cm-deep soil column. We can express $S = f(\theta_s, \theta_r, \alpha, n_{VG}, K_s, \theta_i)$ in closed form (e.g., Moret-Fernández et al., 2017), but experience suggests that this relationship does not always yield accurate estimates of the soil sorptivity. Therefore, we resort to the definition of the sorptivity in Equation 2 and use numerical integration of the HYDRUS-1D simulated $\lambda(\theta)$ curves for horizontal infiltration (no gravity). The penultimate column of Table 1 documents the values of the sorptivity for all our twelve soil types. This concludes the description of the infiltration dataset.

To provide more insights into the hydraulic properties of the soils in our data set, please consider Figure 2, which displays the textural triangle with color coding of each textural class matching (a) the sorptivity, and (b) saturated hydraulic conductivity. Thus, the two triangles map the listed values of S and K_s in Table 1 to their respective textural class. It is evident that soil texture exerts a large control on the sorptivity and saturated hydraulic conductivity. In general, the sorptivity decreases with decreasing sand fraction. We note again that the sorptivities of the silty clay and silty clay loam soils are smaller than their counterpart of the clay soil. This

anomaly somewhat deteriorates the strength of the relationship between the sorptivity, S, and texture of the soil.

Qualitatively similar findings are observed for the saturated hydraulic conductivity of the USDA collection of soils. The color variations of the textural triangle are less pronounced. The saturated hydraulic conductivities of the silty clay, sandy clay, and silty clay loam soils appear rather low in comparison with the documented K_s value of the clay sample. Consequently, these three soils cannot reach the infiltration rate of the clay soil at late times, as is clearly evident from the shape of the cumulative infiltration curves in our dataset. From the textural triangles, we conclude that the silty clay and silty clay loam soils exhibit the lowest values of the sorptivity, S, and saturated hydraulic conductivity, K_s. This explains why from all USDA soils, these two soils infiltrate the least amount of water.

Before we proceed to the section below, we store the infiltration dataset, $\{\tilde{t}_i, \tilde{I}_i\}_{i=1}^n$, of each soil type in two separate vectors, namely, a $n \times 1$ vector, $\tilde{\mathbf{I}} = [\tilde{I}_1 \ \tilde{I}_2 \ \dots \ \tilde{I}_n]$, of cumulative infiltration measurements, and a $n \times 1$ vector of associated print (measurement) times, $\tilde{\mathbf{t}} = [\tilde{t}_1 \ \tilde{t}_2 \ \dots \ \tilde{t}_n]$. The corresponding values of the sorptivity and saturated hydraulic conductivity are referred to as $\tilde{S}$ and $\tilde{K}_s$, respectively. Although we use simulated data in the present analysis, the tilde notation, $\sim$, emphasizes use of observed quantities as precursor to measured infiltration data from laboratory and/or field experiments.

3 | THEORY

In this section, we present the different building blocks of our methodology for assessing the time validity, t_{valid} [L], of Philip's two-term infiltration Equation 5 from measured cumulative infiltration data. As part of this analysis, we also yield estimates of the soil sorptivity, S [L T$^{1/2}$], saturated hydraulic conductivity, K_s [L T^{-1}], and dimensionless coefficient, c. As by-product, we also infer the marginal distribution of coefficient, β, in the infiltration equation of Parlange et al. (1982).

3.1 | The infiltration equation of Parlange

The infiltration equation of Parlange et al. (1982) serves as principal foundation of our methodology. This quasi-exact analytic solution of the water content form of Richards' equation simulates cumulative vertical infiltration, $I(t)$ [L], into a homogeneous soil at uniform initial moisture content:

$$\frac{(K_s - K_i)^2}{S^2}(1 - \beta)t = \frac{(K_s - K_i)[I(t) - K_i t]}{S^2} - \frac{1}{2}\log\left(\frac{1}{\beta}\exp\left\{\frac{2\beta(K_s - K_i)[I(t) - K_i t]}{S^2}\right\} + \frac{\beta - 1}{\beta}\right) \quad (7)$$
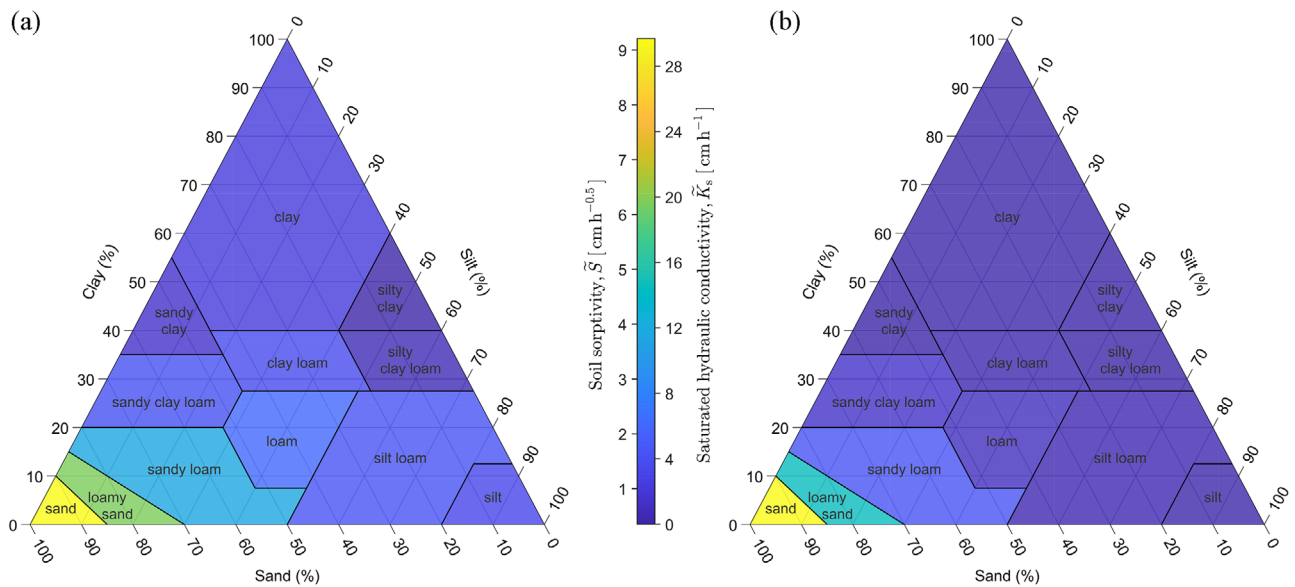
(a)

(b)

FIGURE 2 Textural triangle with the 12 USDA soil types and associated measurements of the (a) sorptivity, $\tilde{S}$, in units of cm h$^{-1/2}$ and (b) saturated hydraulic conductivity, K_s, in cm h^{-1}, using a parula (blue–green–orange–yellow) color map. The colorbar at the right-hand side of both triangles assigns values to the parula color palette

where $t > 0$ [T] is the elapsed time since the start of the infiltration event and $\beta \in (0, 1)$ is a dimensionless integral shape constant (Haverkamp et al., 1990). Equation 7 was generalized to nonponded conditions by Parlange et al. (1985) and Haverkamp et al. (1990) with an expression in explicit form presented by Barry et al. (1995). The coefficient β can be computed as follows (Fuentes et al., 1992; Haverkamp et al., 1994):

$$\beta = 2 - 2\frac{\int_{\theta_i}^{\theta_s} \left[\frac{K(\theta) - K_i}{K_s - K_i} \right] \left(\frac{\theta_s - \theta_i}{\theta - \theta_i} \right) D_w(\theta) d\theta}{\int_{\theta_i}^{\theta_s} D_w(\theta) d\theta} \quad (8)$$

where θ [L^3 L^{-3}] denotes the volumetric soil moisture content at time $t > 0$, $K(\theta)$ [L T^{-1}] and $D_w(\theta)$ [L^2 T^{-1}] signify the unsaturated soil hydraulic conductivity and soil water diffusivity functions, respectively, and $\theta_i \leq \theta \leq \theta_s$. Notwithstanding this theoretical definition for β, its value is difficult to determine from measured infiltration data, as its impact on the $I(t)$ relationship of Equation 7 is visible only at late infiltration times, well beyond the length of most infiltration experiments. It is common practice, therefore, to treat β as a known constant. For example, Haverkamp et al. (1994) obtained $\beta = 0.563$ from application of equation (8), whereas a value of $\beta = 0.6$ is commonly used in the literature (Dohnal et al., 2010; Latorre et al., 2015, 2018; Moret-Fernández et al., 2020; Rahmati et al., 2019). We treat β as an unknown quantity.

Equation 7 has several desirable properties for infiltration modeling and soil hydraulic parameter estimation. First and foremost, Parlange's equation is valid for all infiltration times.

Secondly, as Haverkamp et al. (1994) has shown for a three-dimensional infiltration experiment, the equation is in close agreement with measured data. Lastly, the parameters S, K_s, and β have a sound physical and/or mathematical underpinning, adjustable to the initial and boundary conditions of the infiltration event (Haverkamp et al., 1994; Rahmati et al., 2020). Despite these desirable qualities, Parlange's infiltration Equation 7 has not entered into mainstream use for infiltration modeling and data analysis in lieu of Philip's two-term Equation 5. As Parlange's equation is an implicit solution of the infiltration process, some mathematical skill is required to numerically solve Equation 7 in pursuit of the $I(t)$ relationship.

To simplify practical application of Equation 7, Haverkamp et al. (1994) derived three separate expressions for cumulative infiltration at very short (VS), short (S), and long (L) times, respectively:

$$I^{VS}(t) = S\sqrt{t} \quad (9a)$$

$$I^{S}(t) = S\sqrt{t} + \left[\left(\frac{2 - \beta}{3} \right)(K_s - K_i) + K_i \right] t \quad (9b)$$

$$I^{L}(t) = K_s t - \frac{1}{2(1 - \beta)} \frac{S^2}{K_s - K_i} \log(\beta) \quad (9c)$$

These analytic expressions are much easier to evaluate yet trade difficulties with the numerical solution of Equation 7 with problems about how to establish exact time validities of

Equations 9a–9c and guarantee convergence of the simulated $I(t)$ relationship. Lassabatere et al. (2009) developed time limits for each of the equations and their dependency on soil texture. These limits are only an approximation of the true time validity and require knowledge of the soil texture and values of S and K_s. This undermines practical use. Note that the first term of Equations 9a and 9b is synonymous with the capillary term of Philip's two-term infiltration Equation 5. The second term at the right-hand side of Equation 9b must, therefore, equal Philip's gravity term. Thus, for very short to short infiltration times, we may write

$$c K_s t = \left[\left(\frac{2-\beta}{3}\right)(K_s - K_i) + K_i\right] t \qquad (10)$$

For $K_i = 0$, the expression above simplifies to the following relationship (Moret-Fernández et al., 2017):

$$c = \frac{2}{3} - \frac{1}{3}\beta \qquad (11)$$

between coefficients β and c in the infiltration equations of Parlange et al. (1982) and Philip (1957) (two-term variant), respectively.

In the Supplemental Information S1, we present theory and implementation of an exact and robust numerical solution of Parlange's infiltration equation. This solution considers time, $t \geq 0$ (h), as the independent (explanatory) variable and cumulative infiltration, $I \geq 0$ (cm), as the dependent variable. Our solution builds on the residual form of Equation 7 and uses root finding with the secant method to iteratively find its zero-points. Unlike Newton's method, this procedure does not demand a closed-form expression for the derivative function but uses secant lines to converge the sequence of iterates to the zero-point of Parlange's residual function. Algorithm S1.1 presents a detailed step-by-step recipe of our numerical solution of Equation 7, and Appendix A presents its implementation in MATLAB. This subroutine called Parlange may be executed from the MATLAB command prompt as I = Parlange(eta,t) and is synonymous to a vector-valued function, $\mathbf{I} = \mathbf{f}(\boldsymbol{\eta}, \tilde{\mathbf{t}})$, of the Parlange parameters, $\boldsymbol{\eta} = [S\ K_s\ \beta\ K_i]^\top$, and n measurement times, $\tilde{\mathbf{t}} = [\tilde{t}_1\ \tilde{t}_2\ \dots\ \tilde{t}_n]^\top$. The function returns as output argument the $n \times 1$ vector of cumulative infiltration values, $\mathbf{I} = [I_1\ I_2\ \dots\ I_n]^\top$, of Equation 7. Benchmark experiments (not shown herein) demonstrate that the MATLAB implementation is exact, robust, and computationally efficient requiring only a few milliseconds to complete a 240-h infiltration experiment on a modern desktop computer with print step of 0.1 h.

Parlange's infiltration Equation 7 not only demands an iterative method to solve for its $I(t)$ relationship but also requires use of a search method to estimate its parameters from measured cumulative infiltration data. This amounts to nonlinear regression. The anticipated difficulties with the inference of the coefficient β prompt use of a Bayesian method coupled with the DREAM$_{(ZS)}$ algorithm (Vrugt et al., 2008, 2009; Vrugt, 2016). Such methodology not only returns estimates of the optimum parameter values but simultaneously also assesses their associated uncertainty. Uncertainty quantification is key, as deterministic estimates are difficult to interpret by themselves without knowledge of their underlying confidence intervals.

3.2 | Step 1: Bayesian inverse modeling

We estimate the parameters in Parlange's infiltration equation using Bayesian inference with the DREAM$_{(ZS)}$ algorithm. Bayesian inference allows for an exact description of parameter uncertainty (and other sources of uncertainty) by treating the parameters, η, of Equation 7 as probabilistic variables with joint posterior probability density function, $p(\eta|\tilde{\mathbf{I}})$. This multivariate distribution, the so-called posterior parameter distribution, is the consequence of two antecedents, a prior distribution, $p(\eta)$, which captures our initial degree of beliefs in the values of the model parameters, and a likelihood function, $L(\eta|\tilde{\mathbf{I}})$, which quantifies per the rules of probability theory the level of confidence (= conditional belief) in the parameter values, η, in light of the cumulative infiltration data, $\tilde{\mathbf{I}} = [\tilde{I}_1\ \tilde{I}_2\ \dots\ \tilde{I}_n]^\top$, alone. Bayes' theorem expresses mathematically the fundamental relationship between the prior, conditional, and posterior (= updated) beliefs of the parameters. In the present case, this results in the following formulation:

$$p(\eta|\tilde{\mathbf{I}}) = \frac{p(\eta)L(\eta|\tilde{\mathbf{I}})}{p(\tilde{\mathbf{I}})} \propto p(\eta)L(\eta|\tilde{\mathbf{I}}) \qquad (12)$$

where the denominator, $p(\tilde{\mathbf{I}})$, the so-called evidence or marginal likelihood, acts as a normalizing constant

$$p(\tilde{\mathbf{I}}) = \int_{\mathbf{E}} p(\eta)p(\tilde{\mathbf{I}}|\eta)\mathrm{d}\eta = \int_{\mathbf{E}} p(\eta)L(\eta|\tilde{\mathbf{I}})\mathrm{d}\eta = \int_{\mathbf{E}} p(\eta|\tilde{\mathbf{I}})\mathrm{d}\eta \qquad (13)$$

so that the posterior distribution, $p(\eta|\tilde{\mathbf{I}})$, integrates to unity over the prior (feasible) parameter space, $\eta \in \mathbf{E} \subseteq \mathbb{R}^d$, where d signifies parameter dimensionality. Knowledge of $p(\tilde{\mathbf{I}})$ is strictly necessary for hypothesis testing to select the most plausible infiltration function from a suite of different candidate models deemed valid a priori. If, however, we rely on a single hypothesis, then the denominator, $p(\tilde{\mathbf{I}})$, in Equation 12 is of no particular interest, as all statistical inferences about the parameters of Parlange's infiltration Equation 7 can be made from the unnormalized posterior distribution, $p(\eta|\tilde{\mathbf{I}}) \propto p(\eta)L(\eta|\tilde{\mathbf{I}})$. This necessitates definition of a prior distribution, $p(\eta)$, for the Parlange model parameters, a mathematical form

of the likelihood function, $L(\eta|\widetilde{\mathbf{I}})$, and a method that can infer the posterior distribution, $p(\eta|\widetilde{\mathbf{I}})$.

Before we move on to our choice of prior distribution, we postulate that the hydraulic conductivity, K_i, at the initial moisture content, θ_i, is equal to zero. This assumption is certainly justifiable for our more coarse-textured soils, as their initial moisture contents are relatively low and close to residual saturation (see Table 1). For the more fine-textured soils, the assumption that $K_i = 0$ is questionable; nevertheless, numerical experiments have shown this has a negligible effect on their posterior estimates of S, K_s and β. With $K_i = 0$, Equation 7 simplifies to

$$\left(\frac{K_s}{S}\right)^2 (1-\beta)t = \frac{K_s I(t)}{S^2} - \frac{1}{2}\log\left\{\frac{1}{\beta}\exp\left[\frac{2\beta K_s I(t)}{S^2}\right] + \frac{\beta-1}{\beta}\right\} \tag{14}$$

which leaves us with three unknown parameters, namely, $\eta = [S\ K_s\ \beta]^\top$. Note that this simplification is not given by limitations of our parameter estimation algorithm, as the DREAM$_{(ZS)}$ algorithm can handle a very large number of parameters (Laloy et al., 2015; Linde & Vrugt, 2013; Qin et al., 2018; Zhang et al., 2020). Indeed, a comparison of the marginal prior and posterior distribution of each parameter will convey how much information is available in the calibration data to constrain each parameter. Knowledge of the initial moisture content is important when interpreting the inferred values of S.

3.2.1 | Prior distribution

The prior distribution should encode all the "subjective" knowledge about the Parlange model parameters, $\eta = [S\ K_s\ \beta]^\top$, before collection of the measured cumulative infiltration curve, $\widetilde{\mathbf{I}}$. This distribution, often simply called the prior, expresses one's beliefs about the parameters before the data (also referred to as evidence) are taken into account. In the absence of detailed prior information about the values of S, K_s, and β, we treat all parameter values as equally likely a priori and assign a multivariate uniform prior distribution to the parameter space demarcated by the upper and lower bounds listed in Table 2. This $d = 3$-dimensional hypercube is synonymous to the feasible parameter space, $\mathbf{E}$, and implies a prior density, $p(\eta) = 5 \times 10^{-4}$, so that $\int_E p(\eta) = 1$.

The lower bounds of S, K_s, and β are dictated by physical limits and must be set to zero. Their upper limits, however, are not unambiguous and warrant some discussion. The formal definition of parameter β in Equation 8 implies that $0 < \beta < 2$. This exceeds the interval of $\beta \in (0, 1)$ given by Parlange et al. (1982) but has been used in other recent studies. Note that $\beta \neq 1$, otherwise the left- and right-hand sides of Equation 7 equal zero. The upper bounds of the soil sorptivity and saturated hydraulic conductivity are not as clearly defined and are far more diffuse. We specify rather liberal upper values of

TABLE 2 Description of the parameters of Parlange's infiltration Equation 14 including symbol, units, and lower and upper bounds

Parameter	Description	Unit	Min.	Max.
S	Soil sorptivity	cm h$^{-1/2}$	0	20
K_s	Saturated hydraulic conductivity	cm h^{-1}	0	50
β	Dimensionless coefficient	–	0	2

20 cm h$^{-0.5}$ and 50 cm h^{-1} for S and K_s, respectively, so as to guarantee that our uniform prior, $p(\eta)$, accommodates a diversity of soils. If, for some reason, the upper limits of S and K_s truncate the posterior distribution, $p(\eta|\widetilde{\mathbf{I}})$, then these bounds can always be enlarged.

Note that one can exploit the SWIG database and construct an informative prior for S, K_s, and β for each soil type. Such informative (nonuniform) prior may simplify the inference of β, particularly for infiltration experiments with a limited duration. This warrants further research. The consequence of an uninformative prior is that the posterior parameter distribution, $p(\eta|\widetilde{\mathbf{I}})$, will depend only on the cumulative infiltration data, $\widetilde{\mathbf{I}} = [\tilde{I}_1\ \tilde{I}_2\ \cdots\ \tilde{I}_n]^\top$, through the likelihood function, $L(\eta|\widetilde{\mathbf{I}})$. Indeed, with a uniform prior, the posterior density, $p(\eta|\widetilde{\mathbf{I}})$, of the Parlange parameters, $\eta = [S\ K_s\ \beta]^\top$, will simply equal a constant multiple of 5×10^{-4} of the likelihood, $L(\eta|\widetilde{\mathbf{I}})$, for all $\eta \in \mathbf{E} \subseteq \mathbb{R}^3$. Thus, with an uninformative prior distribution, Bayesian inference reduces to maximum likelihood estimation, but with the important distinction that our framework infers not only the peak of $p(\eta|\widetilde{\mathbf{I}})$, but also its underlying distribution.

3.2.2 | Likelihood function

We are left with the definition of the likelihood function, $L(\eta|\widetilde{\mathbf{I}})$, in Equation 12. The likelihood was designated as mathematical quantity by Sir Ronald Fisher (1934) to measure our degree of belief (confidence) in simulated outcomes. The likelihood principle states that all relevant information about the parameters, η, is contained in the likelihood function for the observed data given the assumed (statistical) model. This offers a self-contained framework for statistical modeling and inference and has become the foundation of modern statistics and probability theory with application to frequentist and Bayesian inference.

In our application, the likelihood (function) quantifies in probabilistic terms the distance between the observed cumulative infiltration data, $\widetilde{\mathbf{I}}$, and its counterpart, $\mathbf{I} = f(\eta, \widetilde{\mathbf{t}})$, simulated by Parlange's infiltration Equation 14 using the parameter values, $\eta = [S\ K_s\ \beta]^\top$, at the n measurement times, $\widetilde{\mathbf{t}} = [\tilde{t}_1\ \tilde{t}_2\ \cdots\ \tilde{t}_n]^\top$. The word *likelihood* is often used loosely in

common speech as synonym for *probability*, yet *probability* is inadequate as mathematical quantity to express our preferences among different outcomes. In practice, the use of the word *probability* is appropriate when describing possible future outcomes for fixed parameter values before data become available. The term *likelihood*, on the contrary, should be used to express the level of confidence for a given outcome (parameter vector) after the infiltration data have become available.

If we wish to quantify the likelihood of a simulated outcome, I_1, in light of an observation, $\tilde{I}_1$, we need to define a probability density function, $f_{\tilde{I}_1}$, for $\tilde{I}_1$. In theory, we could hypothesize any probability distribution for $\tilde{I}_1$, and as a result, many potential formulations of the likelihood function, $L(\eta|\widetilde{\mathbf{I}})$. In practice, however, we often limit our choice to common probability distributions that are easy to manipulate analytically and evaluate numerically. We refer the interested reader to Vrugt and Massoud (2019) for the derivation of a suite of commonly used likelihood functions. In the present application, we make the common assumption that the measurement errors, $\epsilon = [\epsilon_1 \; \epsilon_2 \; \cdots \; \epsilon_n]^\top$, of the $n \times 1$ vector of cumulative infiltration data, $\widetilde{\mathbf{I}}$, are independent (uncorrelated), zero-mean normally distributed with a constant variance, $\sigma_{\tilde{I}}^2$.

Thus, we assume that $\epsilon_j \overset{D}{\sim} \mathcal{N}(0, \sigma_{\tilde{I}}^2)$ for all $j = (1, 2, \ldots, n)$, where $\mathcal{N}(a, b)$ signifies the normal distribution with mean, a, and variance, b and symbol $\overset{D}{\sim}$ means *distributed according to*. Our assumptions lead to the following definition of the likelihood function:

$$L(\eta|\widetilde{\mathbf{I}}) \propto \left\{ \sum_{j=1}^{n} \left[\tilde{I}_j - I(\eta, \tilde{t}_j) \right]^2 \right\}^{-\frac{1}{2}n} \tag{15}$$

where $\tilde{I}_j$ denotes the observed cumulative infiltration at the jth measurement time and $I(\eta, \tilde{t}_j)$ signifies its simulated counterpart at time $\tilde{t}_j$ using Equation 14 with parameter values, $\eta = [S \; K_s \; \beta]^\top$. The summation term between the brackets is the well-known sum of squared residuals (SSR) used in least squares regression methods. Note that $L(\eta|\widetilde{\mathbf{I}})$ is inversely proportional to the SSR; hence, parameter values that minimize the SSR will also maximize the likelihood. As a result, the maximum likelihood solution of the Parlange parameters is synonymous with the least squares solution derived from nonlinear regression methods. Therefore, in the remainder of this paper, the maximum a posteriori density (MAP) solution of $p(\eta|\widetilde{\mathbf{I}})$ is also referred to as least squares solution.

3.2.3 | The DiffeRential Evolution Adaptive Metropolis (DREAM) algorithm

Now that the prior distribution and likelihood function have been defined, what is left is to summarize the posterior distribution, $p(\eta|\widetilde{\mathbf{I}})$, of the Parlange model parameters in Equation 14. As this model is nonlinear in its parameters, the posterior distribution $p(\eta|\widetilde{\mathbf{I}})$ cannot be obtained by analytical means nor by analytical approximation. We must therefore resort to iterative methods that approximate the posterior distribution by generating a large sample from this distribution. In this paper, we approximate the target distribution, $p(\eta|\widetilde{\mathbf{I}})$, using Markov Chain Monte Carlo (MCMC) simulation with the DREAM$_{(ZS)}$ algorithm (Vrugt, 2016; Vrugt et al., 2008, 2009). This multichain MCMC method has found widespread application and use in many different fields of study, and it exhibits excellent sampling efficiencies on complex, high-dimensional, and multimodal target distributions (Laloy et al., 2015; Qin et al., 2018; Volpi et al., 2017;, Zhang et al., 2020; to name a few). A detailed description of this method and its different extensions appears in Vrugt (2016), and interested readers are referred to this paper for more information.

For each soil, we approximate the posterior distribution, $p(\eta|\widetilde{\mathbf{I}})$, of the Parlange parameters, $\eta = [S \; K_s \; \beta]^\top$, using $N = 3$ Markov chains and default settings of the algorithmic variables of the DREAM$_{(ZS)}$ algorithm. In doing so, we use a fixed computational budget of 60,000 Parlange function evaluations and create 20,000 samples in each chain. This number of samples is much larger than required by convergence criteria such as the multivariate scale-reduction factor, $\hat{R}^d$, of Brooks and Gelman (1998), which declared convergence, $\hat{R}^d \leq 1.2$, after just a few thousand chain samples. Hence, we can safely discard the first half of each chain (50% burn-in) and use the last 10,000 samples in each chain to summarize the posterior distribution of the Parlange parameters, S, K_s, and β for each different soil. This amounts to 30,000 posterior parameter vectors, η, and requires about 2 min to complete on a modern desktop computer. The MAP or least squares solution is readily found among these posterior samples by locating the parameter vector with highest posterior density, $p(\eta|\widetilde{\mathbf{I}})$.

3.3 | Step 2: Estimation of c and t_{valid} in Philip's two-term equation

The trivariate posterior distribution of the soil sorptivity S, saturated hydraulic conductivity K_s, and coefficient β of Parlange's infiltration equation serves as input to our second step. Specifically, among the samples of the $N = 3$ Markov chains simulated by the DREAM$_{(ZS)}$ algorithm, we locate the solution that maximizes the posterior density, $p(\eta|\widetilde{\mathbf{I}})$. Due to our choice of prior distribution and likelihood function, the corresponding parameter values are maximum likelihood as well as least squares estimates. We use this wording interchangeably. The least squares parameter values, $\hat{\eta} = [\hat{S} \; \hat{K}_s \; \hat{\beta}]^\top$, of Parlange's infiltration Equation 14 are hard-wired in Philip's

two-term infiltration equation to yield

$$I(t) = \hat{S}\sqrt{t} + c\hat{K}_\mathrm{s}t \qquad (16)$$

This leaves us with two unknowns for each soil, namely, the dimensionless coefficient, c, and the time validity, t_valid, of the above expression. The least squares value, $\hat{c}$, of Equation 16 can be derived by analytic means. For the first m observations, $\widetilde{\mathbf{I}}_m = [\tilde{I}_1\ \tilde{I}_2 \cdots \tilde{I}_m]^\top$, of the n-record of cumulative infiltration measurements, $\mathbf{I}$, we yield

$$\hat{c} = (\mathbf{d}^\top\mathbf{d})^{-1}\mathbf{d}^\top(\widetilde{\mathbf{I}}_m - \hat{S}\widetilde{\mathbf{t}}_m^{1/2}) \qquad (17)$$

where the $m \times 1$ design vector, $\mathbf{d} = [\hat{K}_\mathrm{s}\tilde{t}_1\ \hat{K}_\mathrm{s}\tilde{t}_2 \ldots \hat{K}_\mathrm{s}\tilde{t}_m]^\top$, the $m \times 1$ vector $\widetilde{\mathbf{t}}_m = [\tilde{t}_1\ \tilde{t}_2 \cdots \tilde{t}_m]^\top$ stores the measurement times of $\widetilde{\mathbf{I}}_m$ and $1 \leq m \leq n$. Estimation of the time validity, t_valid, of Philip's two-term infiltration equation now boils down to selection of an optimal value for the integer, m. For $t \leq \tilde{t}_m$, Equation 17 should provide an adequate description of the measured cumulative infiltration curve. For infiltration times, $t > \tilde{t}_m$, Philip's two-term infiltration equation is deemed invalid, and thus its goodness-of-fit is expected to deteriorate substantially.

The Bayesian information criterion (BIC) will help find an optimal trade-off between the quality-of-fit of Equation 17 and the length, m, of the measured infiltration curve. This metric is commonly used for model selection among a finite set of competing hypotheses. The BIC encodes a natural preference for simpler models. This parsimony principle, known as Occam's razor, is traceable to the works of philosophers such as Aristotle (384–322 BC) and Ptolemy (circa AD 90 to circa AD 168) and consistent with requirements of falsifiability in the scientific method of Popper (1992). The BIC is defined as follows in our application:

$$\mathrm{BIC} = -2\log\left[L(\eta|\widetilde{\mathbf{I}}_m)\right] + \log(m) \qquad (18)$$

where $\eta = [\hat{S}\ \hat{K}_\mathrm{s}\ \hat{c}]^\top$ signifies the least squares values of the Parlange parameters, $L(\eta|\widetilde{\mathbf{I}}_m)$ denotes the likelihood of Philip's two-term equation for subset, $\widetilde{\mathbf{I}}_m$, and, again, m is the length of the cumulative infiltration dataset ($m \leq n$). Lower values of the BIC are preferred.

We formalize the above ideas in Algorithm 1, which presents a step-by-step recipe on our use of the BIC for determining the time validity, t_valid, and least squares estimate, $\hat{c}$, of the dimensionless constant, c, of Philip's two-term infiltration (Equation 5). In words, for each length, m, of the subset, $\widetilde{\mathbf{I}}_m$, of cumulative infiltration measurements, we resort to Equation 17 to compute the least squares value of the multiplicative coefficient, c. This value, $\hat{c}$, along with $\hat{S}$ and $\hat{K}_\mathrm{s}$ from Parlange's infiltration equation, enter Philip's two-term infiltration equation and are used to simulate cumula-

tive infiltration, $\mathbf{I}_m$, at measurement times, $\widetilde{\mathbf{t}}_m$. Next, we calculate the likelihood, $L(\eta|\mathbf{I}_m)$, of the simulated infiltration curve, $\mathbf{I}_m$, using Equation 15 and compute the BIC. We execute this recipe for $3 \leq m \leq n$ and look for the value of m that minimizes the BIC. This equals the optimal trade-off between data length and quality of fit and thus is synonymous to the time validity of Philip's two-term infiltration equation.

Algorithm 1. Determination of the time validity, t_valid

Input: Measured cumulative infiltration curve, $\widetilde{\mathbf{I}} = [\tilde{I}_1\tilde{I}_2 \cdots \tilde{I}_n]^\top$ at times, $\widetilde{\mathbf{t}} = [\tilde{t}_1\tilde{t}_2 \cdots \tilde{t}_n]^\top$

Least squares values of sorptivity, $\hat{S} > 0$, and saturated hydraulic conductivity, $K_\mathrm{s} > 0$

Output: Time validity, t_valid, of Equation 14 and corresponding least squares value, $\hat{c}$, of c

  1: **begin**
  2:   Set $\mathrm{BIC}_1 = 10^{10}$, $\mathrm{BIC}_2 = 10^{10}$, $\hat{c}_1 = 0$, and $\hat{c}_2 = 0$
  3:   **for** $m \leftarrow 3$ to n **do**
  4:     Define cumulative infiltration subset, $\widetilde{\mathbf{I}}_m = [\tilde{I}_1\ \tilde{I}_2\ \cdots\ \tilde{I}_m]^\top$, at $\widetilde{\mathbf{t}}_m = [\tilde{t}_1\ \tilde{t}_2\ \cdots\ \tilde{t}_m]^\top$
  5:     Define the $m \times 1$ design vector, $\mathbf{d}$, of coefficient c, that is, $\mathbf{d} = [\hat{K}_t\tilde{t}_1\ \hat{K}_t\tilde{t}_2\ \cdots\ \hat{K}_t\tilde{t}_m]^\top$
  6:     Compute the least squares value, $\hat{c}_m$, of coefficient c, $\hat{c}_m = (\mathbf{d}^\top\mathbf{d})^{-1}\mathbf{d}^\top(\widetilde{\mathbf{I}}_m - \hat{S}\widetilde{\mathbf{t}}_m^{1/2})$
  7:     Evaluate Philip's two-term Equation 16 at $\widetilde{\mathbf{t}}_m$ using $\eta = [\hat{S}\ \hat{K}_\mathrm{s}\ \hat{c}_m]^\top$
  8:     Compute the likelihood, $L(\eta|\widetilde{\mathbf{I}}_m)$, of the simulatedinfiltration data, $\mathbf{I}_m$, using Equation 15
  9:     Compute the Bayesian information criterion, $\mathrm{BIC} = -2\log[L(\eta|\widetilde{\mathbf{I}}_m)] + \log(m)$
  10: **end for**
  11: Find the index, $\hat{m}$, of the minimum BIC, thus, $\hat{m} = \arg\min_{1 \leq m \leq n}\mathrm{BIC}(m)$
  12: Define the time validity, $t_\mathrm{valid} = \tilde{t}_{\hat{m}}$
  13: **return** t_valid and $\hat{c}_{\hat{m}}$
  14: **end**

4 | RESULTS AND DISCUSSION

In this section, we present the results of our framework for the 12 different soil types considered in our analysis. We first present the results of Step 1 of our methodology, after which we move on to our findings for the second step.

4.1 | Results of Step 1: Parlange's equation

Figure 3 displays time series plots of the HYDRUS-1D simulated cumulative infiltration data (red circles) of each soil type and their simulated counterparts (solid blue line) of the infil-
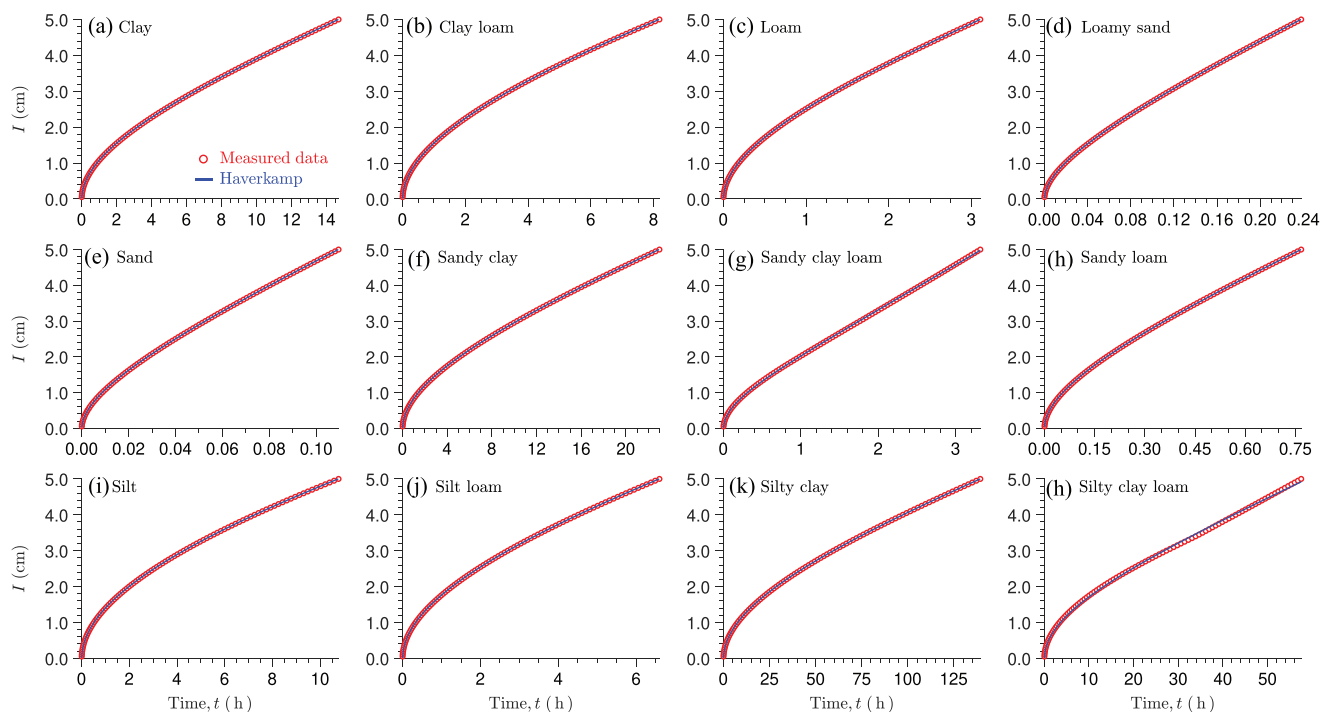
FIGURE 3 Comparison of observed (red dots) and simulated cumulative infiltration, I, data using the semi-implicit equation of Parlange et al. (1982) for the 12 different USDA textural classes. Each dataset is composed of $n = 100$ measurements and differs in duration as the cumulative infiltration is limited to 5 cm

tration equation of Parlange with least squares value of S, K_s, and β derived from Bayesian analysis using the DREAM$_{(ZS)}$ algorithm. The simulated cumulative infiltration is in excellent agreement with the measured data. For all soil types, the solid blue line goes nearly perfectly through the measured $(\tilde{t}, \tilde{I})$ data pairs. This result may not come as a complete surprise, as both the measured and simulated data equal a solution of Richards' equation, albeit in numerical and analytic form and with and without specification of the initial moisture content, respectively.

To provide insights into the corresponding estimates of the Parlange parameters, please consider Figure 4, which presents marginal posterior distributions of the soil sorptivity, S, in cm h$^{-1/2}$, saturated hydraulic conductivity, K_s, in cm h^{-1}, and unitless coefficient, β, for a representative group of five soils including (a) clay, (b) clay loam, (c) sand, (d) silt loam, and (e) silty clay loam. The relative frequencies on the y axis are scaled between 0 and 1 to yield a common empirical density for each parameter and soil type. The least squares value of each parameter is separately indicated in each graph using a red cross. The Parlange parameters, S, K_s, and β, appear well defined by calibration against the measured cumulative infiltration data. The histograms occupy only a small region interior to their uniform prior distributions. This is a testament to the information content of the cumulative infiltration data. The posterior marginal distributions of S, K_s, and β are generally well described by a normal distribution with mean

that coincides with their respective least squares estimates and small dispersion. The only exception is parameter β for silty clay loam (Figure 4E3). Its histogram is truncated at two by the prior distribution and, consequently, differs markedly from normality. A similar result is observed for sandy clay loam (not shown). Our numerical solution of Parlange's infiltration equation detailed in Supplemental Section S1 and Appendix A accommodates β values larger than 2. Thus, we temporarily lift the restriction that $0 < β < 2$ and use an upper bound, $β = 5$, in our next trials with the DREAM$_{(ZS)}$ algorithm. The use of such enlarged prior for β only changes the posterior distribution of the sandy clay loam and silty clay loam soils. The marginal distributions of their β values (not shown) now become Gaussian as well (as all other histograms) with posterior means of about 3.5 and 4.5, respectively, and small variance. The desire of the posterior β values of sandy clay loam and silty clay loam to exceed 2 defies the mathematical–physical definition of β in Equation 8. Therefore, we revoke that $0 < β \leq 2$ and classify sandy clay loam and silty clay loam as *dissonant* soils in the remainder of this paper.

Table 3 documents summary statistics of the posterior parameter distribution, $p(\eta|\tilde{\mathbf{I}})$, sampled with the DREAM$_{(ZS)}$ algorithm. Specifically, for each soil type, we list the posterior mean, median, and standard deviation of S, K_s, and β. This table reiterates the main findings of Figure 3. The Parlange parameters are well defined with posterior standard deviations that appear rather small. The total cumulative infiltra-

TABLE 3 Summary statistics of the DREAM$_{(ZS)}$–derived posterior distribution, $p(\eta|\widetilde{\mathbf{I}})$, of the parameters, $x = [S\ K_s\ \beta]^\top$, of Parlange's infiltration equation for the twelve different soils considered in our analysis

Soils	S			K_s			β		
	Mean	Median	SD	Mean	Median	SD	Mean	Median	SD
	—cm h$^{-1/2}$—			—cm h^{-1}—					
Clay	1.041	1.041	0.004	0.213	0.213	0.002	1.636	1.636	0.047
Clay loam	1.491	1.491	0.005	0.306	0.307	0.006	1.500	1.500	0.063
Loam	2.267	2.267	0.008	0.969	0.969	0.009	1.508	1.508	0.049
Loamy sand	6.316	6.317	0.023	15.260	15.262	0.078	0.837	0.837	0.031
Sand	9.326	9.326	0.035	31.866	31.879	0.242	0.703	0.704	0.035
Sandy clay	0.799	0.799	0.003	0.136	0.136	0.001	1.366	1.367	0.050
Sandy clay loam	1.698	1.698	0.004	1.261	1.261	0.002	1.988	1.992	0.012
Sandy loam	3.907	3.907	0.005	4.443	4.443	0.011	1.053	1.053	0.014
Silt	1.381	1.381	0.005	0.204	0.205	0.006	1.759	1.760	0.070
Silt loam	1.703	1.703	0.006	0.377	0.378	0.007	1.686	1.687	0.064
Silt clay	0.353	0.353	0.001	0.021	0.021	0.000	1.698	1.698	0.048
Silty clay loam	0.518	0.518	0.002	0.058	0.058	0.001	1.975	1.984	0.026

Note. Parameter *S* is sorptivity, K_s is saturated hydraulic conductivity, and β is a coefficient.
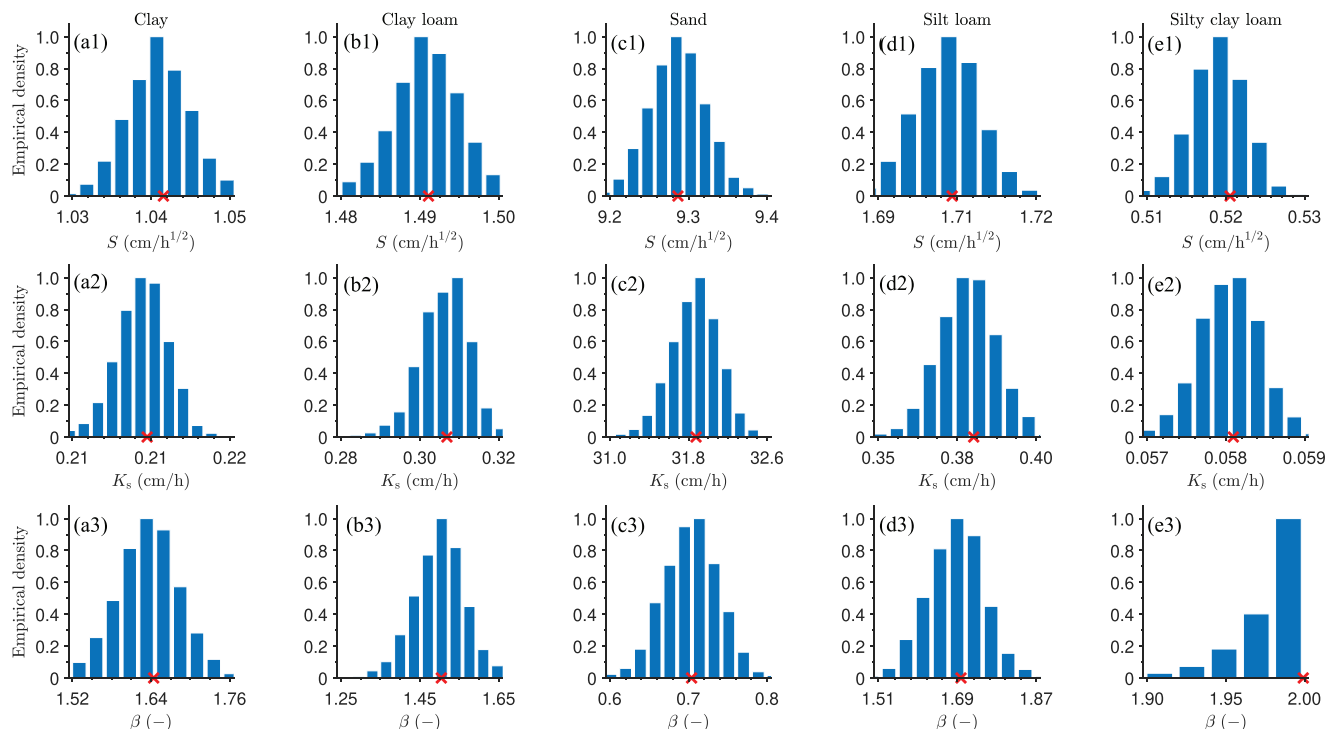
FIGURE 4 Histograms of the marginal posterior distribution of the parameters sorptivity (S), saturated hydraulic conductivity (K_s), and β coefficient of Parlange's semi-implicit infiltration Equation 14 for a representative set of five soils, including (a) clay, (b) clay loam, (c) sand, (d) silt loam, and (e) silty clay loam. The least squares values of the parameters are separately indicated in each graph with the red cross symbol

tion of 5 cm is more than enough for each soil type to warrant a precise determination of its sorptivity, saturated hydraulic conductivity, and dimensionless coefficient, β, in Parlange's infiltration Equation 14. Whether the posterior estimates of S and K_s are accurate or not will soon be investigated. Note that sandy clay loam suffers a similar problem with its β value as silty clay loam, our other dissonant soil. Fortunately, as we will demonstrate soon, the truncation of β at a value of 2 hardly affects the accuracy of the inferred S and K_s values.

Next, we investigate the induced correlation structure between the posterior samples of the Parlange parameters. Figure 5 presents scatter plots of the bivariate posterior samples of (1) (S, K_s), (2) ($S, β$) and (3) ($K_s, β$) for the (a) clay, (b) clay loam, (c) sand, (d) silt loam, and (e) silty clay loam soils. The dashed black line presents the fit of a linear regression model to the scattered samples, and the red cross portrays the least squares solution of each parameter pair. The bivariate scatter plots of the sampled posterior parameter values demonstrate the presence of considerable parameter correlation. Indeed, for all but our two dissonant soils (sandy clay loam not shown), the Parlange parameter pairs (S, K_s), ($S, β$), and ($K_s, β$) exhibit an almost linear relationship with strength of the correlation that depends on the spread of the samples around the regression line and results in correlation coefficients that range between .80 and .95 (see Table 4). Thus, if a small increment of the sorptivity is met by a proportionate positive perturbation to parameters K_s or β, then the cumula-

TABLE 4 Pairwise linear correlation coefficients between the parameters of Parlange's infiltration equation for each of the soil types considered herein

	Parameter pairs		
Soil type	**(S, K_s)**	**($S, β$)**	**($K_s, β$)**
Clay	0.826	0.971	0.932
Clay loam	0.858	0.959	0.966
Loam	0.827	0.964	0.943
Loamy sand	0.817	0.954	0.949
Sand	0.849	0.950	0.970
Sandy clay	0.837	0.964	0.949
Sandy clay loam	−0.663	0.553	0.120
Sandy loam	0.815	0.955	0.947
Silt	0.858	0.962	0.963
Silt loam	0.851	0.964	0.957
Silt clay	0.842	0.969	0.945
Silty clay loam	−0.671	0.485	0.208

Note. The correlation coefficients are derived from the posterior samples of the DiffeRential Evolution Adaptive Metropolis (DREAM) algorithm Parameter S is sorptivity, K_s is saturated hydraulic conductivity, and β is a coefficient.

tive infiltration simulated by the Parlange infiltration equation may not change much, resulting in an approximately similar value of the likelihood, $L(\eta|\widetilde{\mathbf{I}})$. The truncated marginal distribution of β for the silty clay loam and sandy clay loam soils is
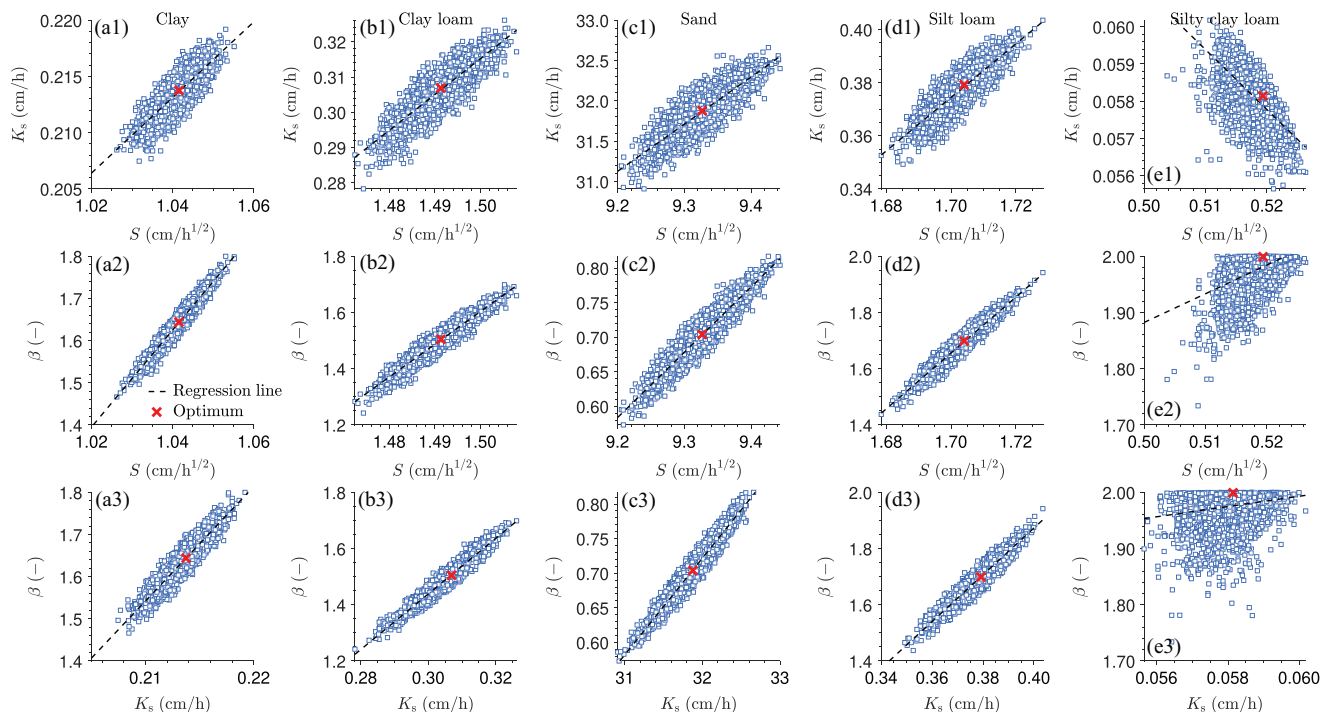
FIGURE 5 Scatter plots of the bivariate posterior samples of the parameter pairs, (1) (S, K_s), (2) (S, β) and (3) (K_s, β) of the Parlange infiltration Equation 14 for a representative group of five soil types, including (a) clay, (b) clay loam, (c) sand, (d) silt loam, and (e) silty clay loam. Parameter S is sorptivity, K_s is saturated hydraulic conductivity, and β is a coefficient. The dashed black line characterizes the fit of a linear regression function to the sampled data pairs. The red cross signifies the least squares solution of the Parlange parameters

responsible for an enhanced dispersion of the posterior samples along the regression line. This increased spread not only reduces considerably the strength of the relationship between the Parlange parameters, S, K_s and β, but also changes to a negative value the correlation between S and K_s (see Figure 4E1).

The posterior correlation structure among S, K_s, and β of Parlange's infiltration equation signals a warning. We should not expect a method that can simultaneously determine the time validity, t_{valid}, and the parameters, S, K_s, and c, of Philip's two-term infiltration equation. No method and/or framework would allow us to do this with confidence. If nothing else, we may be able to determine the product of c and K_s, but their individual values are ill defined in calibration against cumulative infiltration data. This testifies to the need of our two-step inference method using Parlange's infiltration function as a vehicle for the soil sorptivity and saturated hydraulic conductivity.

Finally, we conclude the results of our first step with a pairwise comparison of the observed and least squares (maximum likelihood) estimates of the (a) soil sorptivity, S, and (b) saturated hydraulic conductivity, K_s (see Figure 6). For completeness, Table 5 lists the maximum likelihood values of S and K_s including corresponding estimates of $\hat{\beta}$. The maximum likelihood estimates of $\hat{S}$ and $\hat{K}_s$ derived from the DREAM$_{(ZS)}$ algorithm are in excellent agreement with

TABLE 5 Maximum likelihood estimates of the parameters, sorptivity (S), saturated hydraulic conductivity (K_s), and β coefficient, of Parlange's infiltration equation derived from the joint samples of the Markov chains of the DREAM$_{(ZS)}$ algorithm

Soil type	$\hat{S}$	$\hat{K}_s$	$\hat{\beta}$
	cm h$^{-1/2}$	cm h^{-1}	
Clay	1.042	0.214	1.644
Clay loam	1.491	0.307	1.505
Loam	2.267	0.969	1.507
Loamy sand	6.315	15.261	0.836
Sand	9.327	31.877	0.704
Sandy clay	0.799	0.136	1.363
Sandy clay loam	1.700	1.261	2.000
Sandy loam	3.907	4.443	1.053
Silt	1.381	0.205	1.766
Silt loam	1.704	0.379	1.699
Silt clay	0.353	0.021	1.702
Silty clay loam	0.519	0.058	1.999

Note. The "measured" values of the soil sorptivity, S, and saturated hydraulic conductivity, K_s, are listed in Table 1.

their measured counterparts listed in the last two columns of Table 1. Indeed, the data pairs of the 12 soil types lie almost exactly on the 1:1 line that is going from left to right
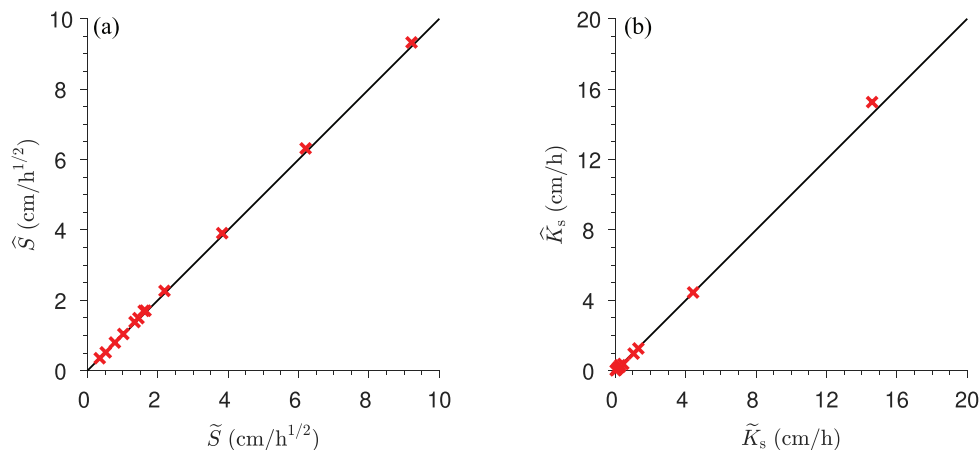
FIGURE 6 Scatter plots of the observed, ∼, and estimated, ^, values of the (a) soil sorptivity, S, in cm h$^{-1/2}$ and (b) saturated soil hydraulic conductivity, K_s, in units of cm h^{-1}. The solid black line characterizes the 1:1 relationship between the measured and estimated quantities

across the graphs. Thus, the maximum likelihood parameter values of Parlange's infiltration equation do not only describe accurately the measured infiltration data but also match their observed values. Setting $K_i = 0$ in Parlange's infiltration equation does not seem to deteriorate the accuracy of the inferred sorptivities and saturated soil hydraulic conductivities. The β values listed in Table 4 of Lassabatere et al. (2009) for sand, loam, silt, and silt loam are in good agreement with our estimates for these soil types.

Now, the MAP values of the sorptivity, S, and saturated hydraulic conductivity, K_s, are known for each soil type, we can exploit this knowledge in Step 2 of our methodology and determine the multiplicative coefficient, c, and time validity, t_{valid}, of Philip's two-term infiltration Equation 5.

4.2 | Results of Step 2: Time validity of Philip's two-term equation

Figure 7 visualizes the results of Algorithm 1 and displays traces of the BIC (in blue) and least squares value of the multiplicative coefficient, c (in green), of Philip's two-term infiltration equation for all 12 USDA soil types. All graphs have the exact same vertical axes (in blue and green) with tick labels listed only for the three figures in the leftmost column. The solid red dot at the intersection of the dashed red line and the x axis equals the time validity, t_{valid}, of Philip's two-term infiltration equation. The different traces of the BIC and $\hat{c}$ highlight several important findings. In the first place, notice the strong similarities in the BIC and $\hat{c}$ traces of the different soil types. The BIC decreases rapidly at early times of infiltration, then assumes rather similar values at intermediate times before increasing again towards the end of the infiltration experiment. The characteristic banana-shaped form of each BIC trace is the net result of two competing model evaluation criteria, namely, the length of the data set, m, in Equa-

tion 18, and the quality of fit (likelihood) of Philip's two-term infiltration equation. The BIC will go down if a unit increment of the length of the cumulative infiltration dataset is met by a sufficiently large increase in the likelihood, $L(\eta|\widetilde{\mathbf{I}}_m)$. With exception of the loamy sand and sandy loam soils (see Figures 7D, H), the least squares values of the multiplicative coefficient, c, drop almost instantly to values between 0.05 and 0.30 at very early infiltration times and then increase again with each length increment of the cumulative infiltration dataset. Secondly, the BIC traces of the different soil types exhibit a single well-defined minimum. This characteristic of the BIC metric is crucially important in our search for an optimum model complexity and allows for an accurate determination of the time validity of Philip's two-parameter infiltration equation. Indeed, the minimum BIC presents an optimal trade-off between the length of the cumulative infiltration data set and the quality of fit of Philip's two-term infiltration equation.

In the third place, notice that the time validity of each soil is well within the time required to infiltrate 5 cm of water. Whereas silty clay and silty clay loam warrant an infiltration experiment of about 2–3 d, most other soils need only a few hours. Furthermore, the inferred time validities correlate with soil texture. This may help develop practical guidelines on when to use Philip's two-term equation. Lastly, the values of coefficient c at $t = t_{valid}$ are significantly smaller than one and well within the ranges reported in the literature. This inspires further confidence in our methodology and will be discussed below.

Table 6 reports the least squares values of coefficient, c, and corresponding estimates of t_{valid} for Philip's two-term infiltration equation. The last column lists the characteristic time, t_{char}, of Equation 6 of Philip (1957). The optimum value of coefficient c ranges between 0.3 and 0.5 for soils with a relatively large sand fraction to values of 0.20–0.25 for soils with a high loam and clay content and values of about 0.15–0.20
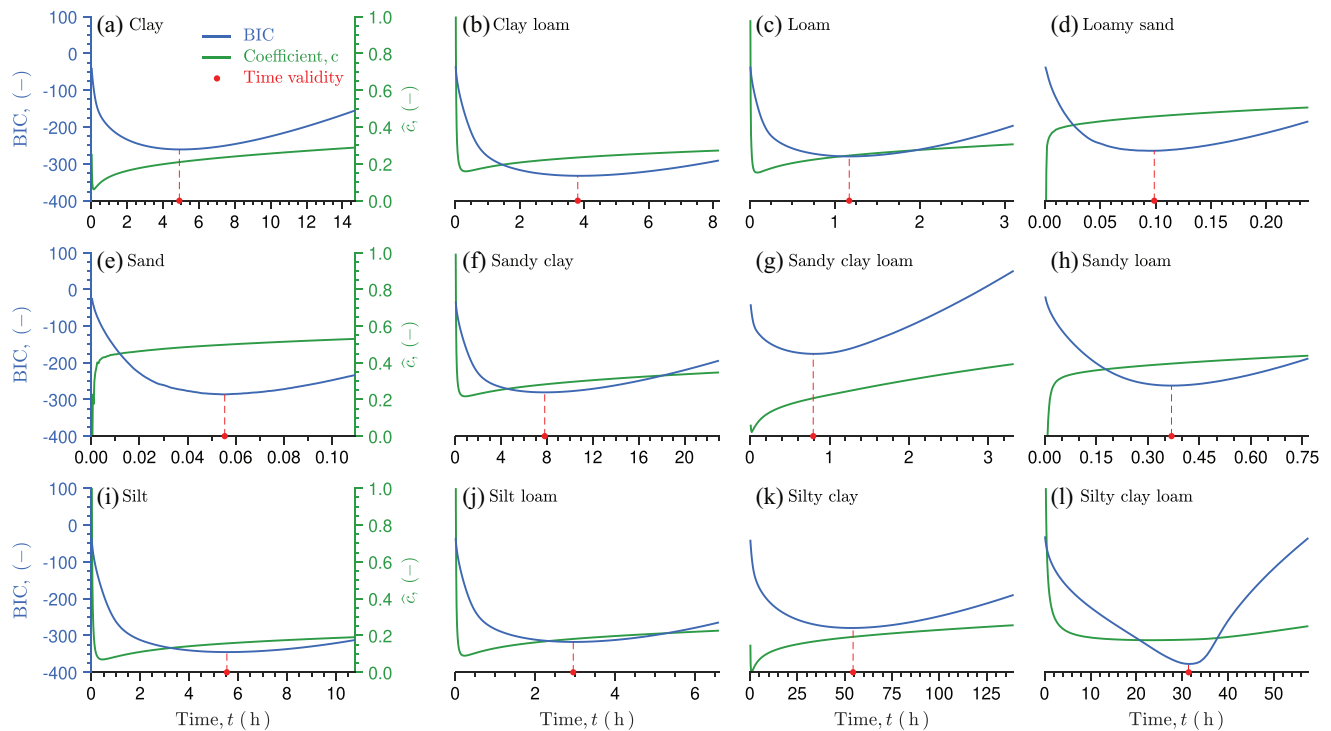
FIGURE 7 Relationship between the Bayesian information criterion, BIC (in blue) and least squares value, $\hat{c}$ (in green), of the multiplicative coefficient, c, of Philip's two-term infiltration Equation 5 as function of the length of the infiltration experiment for all 12 soil types considered in our analysis. The graphs in Columns 2, 3, and 4 share the same vertical axis (left and right) as Graphs a, e, and i in the leftmost column. The vertical dashed red line pinpoints the minimum of the BIC. The solid red dot at the intersection of the red line and the x axis signifies the time validity of Philip's two-term infiltration equation

TABLE 6 Least squares value of the multiplicative coefficient, c, with corresponding estimates of the time validity, t_{valid}, of Philip's two-term infiltration equation

Soil type	$\hat{c}$	t_{valid}	t_{char}
		—h—	
Clay	0.210	4.909	23.745
Clay loam	0.235	3.799	23.616
Loam	0.245	1.169	5.471
Loamy sand	0.458	0.099	0.171
Sand	0.498	0.055	0.086
Sandy clay	0.282	7.800	34.464
Sandy clay loam	0.207	0.795	1.818
Sandy loam	0.395	0.369	0.773
Silt	0.157	5.541	45.451
Silt loam	0.181	2.949	20.197
Silt clay	0.192	54.454	288.160
Silty clay loam	0.178	31.425	79.799

Note. The last column lists the characteristic time, t_{char}, derived from Philip (1957) using Equation 6.

for silty soils. These values are not uncommon for the different soil types. We can confirm these estimates by application of our method to the soils of the SWIG database. The time validity of each soil type is much smaller than the characteristic time, t_{char}, of Philip (1957) and the gravity time, t_{grav}, of the characteristic time method of Rahmati et al. (2020). This reiterates the importance of an assumption-free and data-driven methodology for assessing the time validities of infiltration models. Nevertheless, t_{valid} and t_{char} (and for that matter t_{grav}) exhibit a strong linear relationship with correlation coefficient that exceeds .95.

We have focused our attention on an assessment of the multiplicative coefficient, c, and the time validity, t_{valid}, of Philip's two-term equation without recourse to an assessment of the quality of fit of this infiltration equation. Figure 8 compares measured (red dots) and simulated infiltration data (solid blue line). Measured data beyond t_{valid} are separately displayed in light red. Philip's two-term equation is in excellent agreement with the measured infiltration data for $t \leq t_{valid}$. This is true for all soil types. For infiltration times larger than t_{valid}, Philip's two-term equation is known to be deficient in describing the infiltration process, and the simulated curves deviate more and more from the measured data. The cumulative infiltration at $t = t_{valid}$ ranges between 2.5 to 3.2 cm but is limited to about 1.8 cm for sandy clay loam. Thus, a cumulative infiltration of about 2.8–3.0 cm may serve as a reasonable proxy for the time validity of Philip's two-term equation. In fact, at $t = t_{valid}$ the soil has reached an approximately constant rate of infiltration.
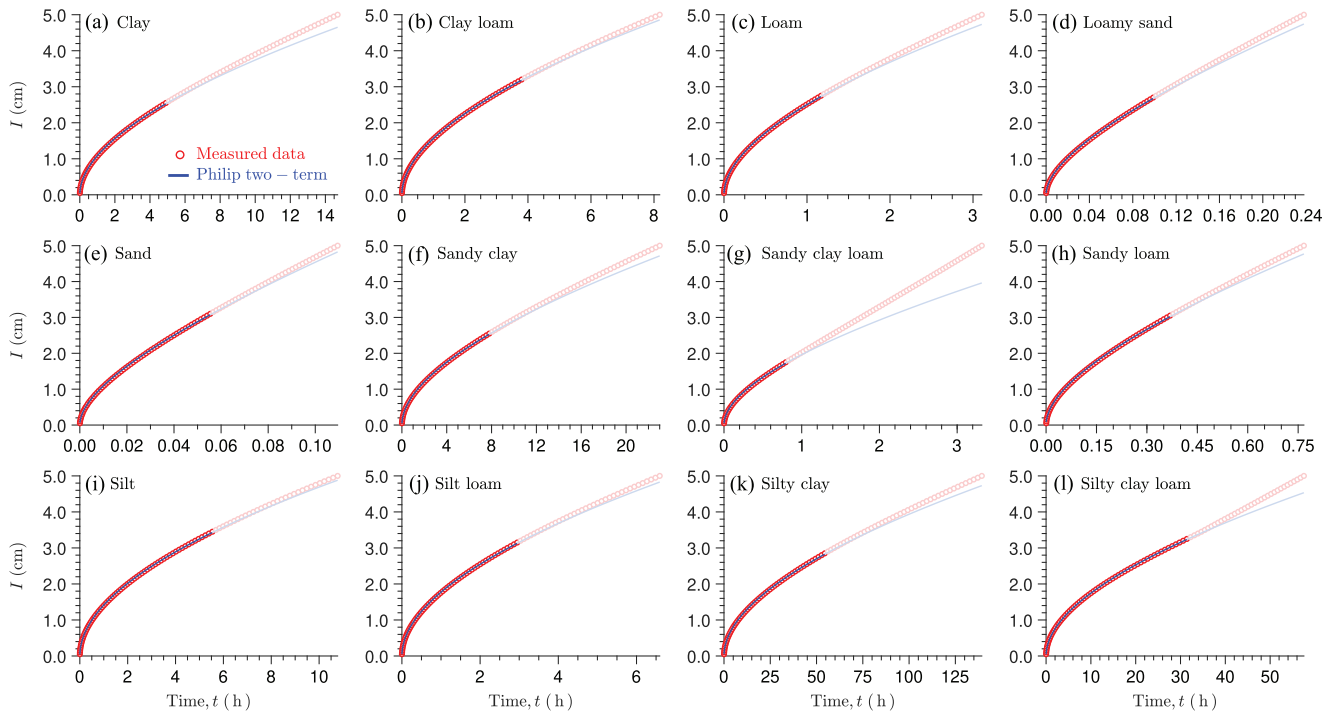
FIGURE 8 Comparison of observed (red dots) and simulated cumulative infiltration, I, using Philip's two-term infiltration Equation 5 with least squares values of the sorptivity, S, and saturated hydraulic conductivity, K_s, derived from Parlange's equation (Step 1, see Table 5) and multiplicative coefficient, c, and time validity, t_{valid}, from Step 2 of our methodology (e.g., see Table 6). Each graph corresponds to a different soil type. Measured cumulative infiltration data beyond the time validity of Philip's two-term equation are displayed with a tint of red
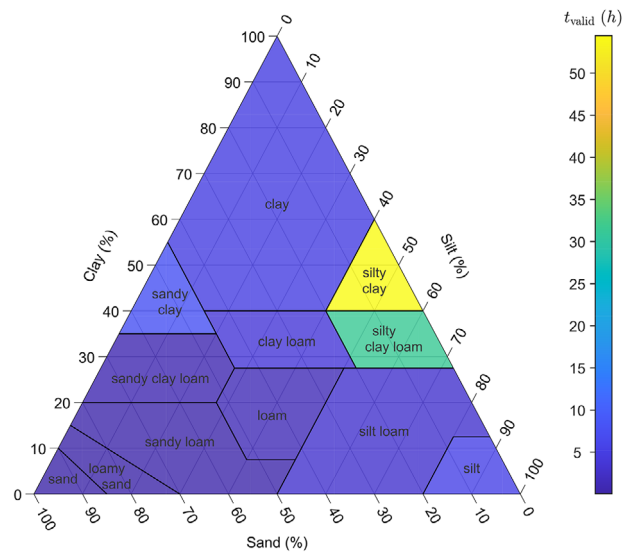

FIGURE 9 Textural triangle of the 12 USDA soil types with color coding of the least squares values of the time validity, t_{valid}, of Philip's two-term infiltration equation. The colorbar assigns values to the palette of the time validity

Figure 9 links the time validity of Philip's two-term infiltration equation to soil texture using color coding for each soil type. The rather large values of t_{valid} for silty clay and silty clay loam suppress the subtle color variations in the time validity of the other soil types. Along with Table 6 it is not too difficult to discern a trend in the inferred time validities of Philip's two-term infiltration equation. Indeed, the finer the texture of the soil the larger the value of t_{valid} will be. We may turn this trend into a regression equation to anticipate the time validity of Philip's two-term expression for other soils, yet this demands textural information. If, however, the interest is only in the hydraulic properties of the soil, then Parlange's infiltration equation will suffice to back out the soil's sorptivity and saturated hydraulic conductivity.

Next, we present the texture triangle with color of each soil type proportional to the maximum likelihood value of the multiplicative coefficient c (see Figure 10). The colored triangle discloses a pattern in the optimum value of c in Philip's two-term infiltration equation. In general, the value of c decreases along two of the principal axes of the triangle, namely, the percentages of sand and clay. Not all soil types honor this relationship—for example, sandy clay loam, one of our two dissonant soils.

Now that we completed Step 2, we can investigate the relationship between the least squares value of coefficient c in Philip's two-term infiltration equation, and the maximum likelihood value of β in Parlange's infiltration equation. Figure 11 visualizes this relationship.

The dashed black line plots the identity, $c = (2/3) - (1/3)\beta$, of Equation 11, valid for very short to short infiltration
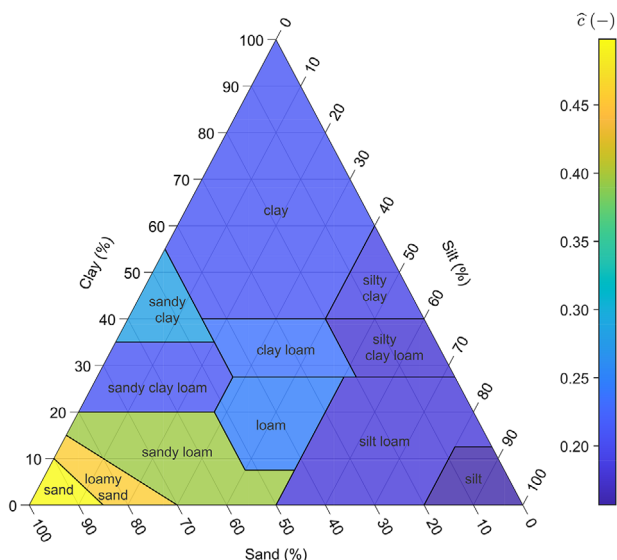
FIGURE 10 Textural triangle of the 12 USDA soil types with projection of the least squares values of the multiplicative dimensionless coefficient, c, of Philip's two-term infiltration equation. The colorbar assigns values to coefficient, c
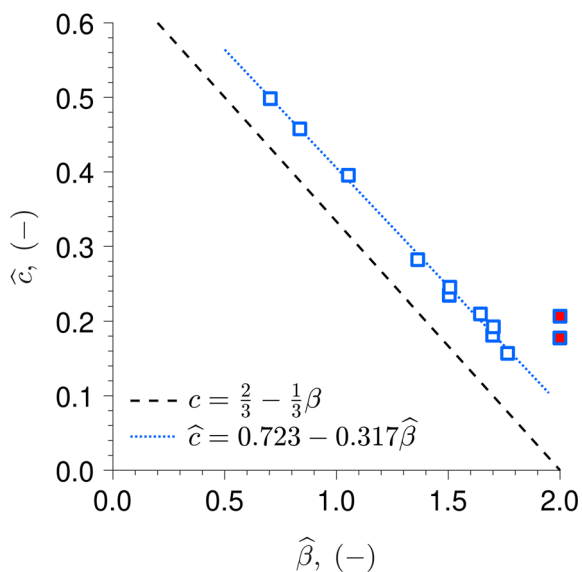

FIGURE 11 Comparison of the DREAM$_{(ZS)}$–derived maximum likelihood value of parameter β of Parlange's semi-implicit infiltration equation (Step 1) and the least squares value of coefficient c of Philip's two-term infiltration equation derived in Step 2 of our methodology (values tabulated in Table 6). The solid black line portrays the theoretical relationship of Equation 11 between β and c, valid at short infiltration times. The two red colored data points correspond to our dissonant soils, sandy clay loam, and silty clay loam, whose histograms of β are truncated by the prior distribution (see Figures 4E3, 5E2, and 5E3). The dotted blue line equals the least squares fit through the data, but without the two $(\hat{\beta}, \hat{c})$ pairs of the dissonant soils

times. The data points of sandy clay loam and silty clay loam are marked in red as their respective $\hat{\beta}$ values have been truncated at 2. Thus, we discard the $(\hat{\beta}, \hat{c})$ data pairs of these two dissonant soils in our subsequent analysis. The $(\hat{\beta}, \hat{c})$ scatter plot illustrates several interesting findings. First and foremost, the data pairs appear to lay on a line, confirming the presence of a linear relationship between the dimensionless coefficients β and c. Secondly, the linearity of the β(c) relationship of Equation 11 appears to extend beyond early infiltration times. Third, the $(\hat{\beta}, \hat{c})$ data pairs do not match perfectly the dashed black line, valid for very short to short infiltration times. Linear least squares of the $(\hat{\beta}, \hat{c})$ data without the two dissonant soils produces the relationship $c = 0.723 - 0.317\beta$ between coefficients β and c of Parlange and Philip's infiltration equations, respectively. The slope and intercept of this regression function (dotted blue line) are only marginally different from their counterparts of Equation 11; nevertheless, they extend up to the time validity of Philip's two-term infiltration equation. Thus, the identity $c = 0.723 - 0.317\beta$ produces an almost perfect match with the maximum likelihood values of Parlange's β coefficient derived from the DREAM$_{(ZS)}$ algorithm in Step 1 of our methodology. This new identity is approximately similar to

$$c = \frac{1}{\sqrt{5}}\psi - \frac{1}{\pi}\beta \qquad (19)$$

where $\psi = (1/2) + (1/2)\sqrt{5} \approx 1.6180$ denotes the so-called golden ratio.

5 | IMPLICATIONS

The scatter plot in Figure 11 confirms the presence of a linear $c(\beta)$ relationship within the time validity of Philip's two-term infiltration equation. We can take advantage of this identity to simplify our methodology. After Step 1 is completed, we can turn the sampled posterior values of β into a marginal distribution of the dimensionless coefficient c, hereafter referred to as c_β, using the relationship of Equation 19. Next, we can evaluate Philip's two-term infiltration equation for each augmented vector, $\eta^+ = [S\,K_s\,\beta\,c_\beta]^\top$, of posterior parameter values and compute the 2.5 and 97.5% simulation uncertainty ranges at each measurement time.

Figure 12 presents the marginal distribution of c_β and displays the associated 95% prediction ranges of Philip's two-term infiltration equation for (a) clay, (b) clay loam, (c) sand, (d) silt loam, and (e) silty clay loam. Measured infiltration data beyond t_{valid} use a different red tint. The most important results are as follows. The marginal distribution of c_β centers on $\hat{c}$ derived from Step 2 of our methodology and is well
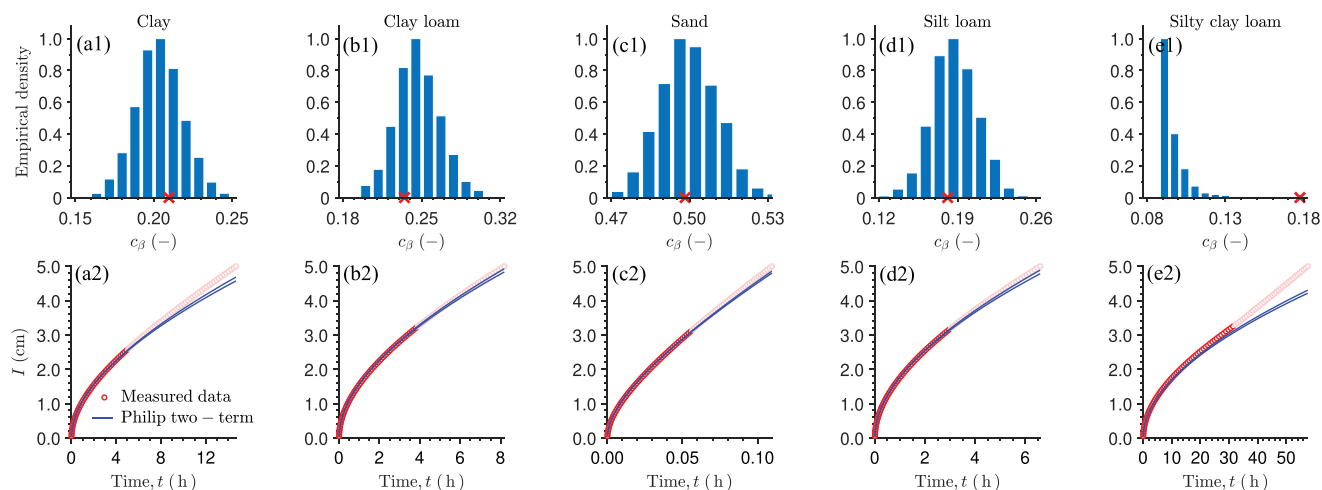
FIGURE 12 Top panel: Marginal distribution of the multiplicative coefficient, c, of Philip's two-term infiltration equation derived from Equation 19, for a representative group of five soil types, including (a) clay, (b) clay loam, (c) sand, (d) silt loam, and (e) silty clay loam. The least squares values of c from Step 2 of our methodology are separately indicated in each graph with the red cross symbol. Bottom panel: Comparison of observed (red dots) and 95% prediction ranges of the cumulative infiltration (I, solid blue lines) simulated with Philip's two-term infiltration Equation 5 using the posterior samples of the sorptivity, S, saturated hydraulic conductivity, K_s, and coefficient, c_β, derived from Parlange's equation in Step 1 of our methodology. Thus, the two infiltration curves correspond to the 2.5 and 97.5% prediction quantiles derived from the posterior samples. Measured data beyond the time validity of Philip's two-term equation inferred in Step 2 of our methodology are displayed with a tint of red

described by a normal distribution for all but the two dissonant soils. The histogram of c_β for silty clay loam (Figure 12E1) suffers from truncation at $\beta = 2$, resulting in a skewed distribution with right tail. Its least squares value appears outside the marginal distribution of c_β as the $(\hat{\beta}, \hat{c})$ data pairs of the two dissonant soils were omitted in the computation of the $c(\beta)$ relationship of Equation 19. This discrepancy between $\hat{c}$ and the histogram of c_β values causes the 2.5 and 97.5% prediction quantiles of Philip's two-term equation for the silty clay loam soil to deviate from the measured infiltration data before t_{valid} is reached. Upon closer inspection of the residuals, one would anticipate a time validity for silty clay loam on the order of 7–8 h. For the other four soils, Philip's 2.5 and 97.5% prediction quantiles (Figure 12A2–D2) match perfectly the measured infiltration data for $0 \leq t \leq t_{valid}$. As expected, at larger infiltration times, the two prediction quantiles deviate systematically from the measured $(\tilde{t}, \tilde{I})$ data pairs.

In Step 1, we made the assumption of normally distributed infiltration data measurements errors. The variance of the measurement errors was integrated out to yield a simple formulation of the likelihood function. If we specify the cumulative infiltration measurement error up front, then we can use a χ^2 test to turn each residual of Philip's infiltration equation and the measured cumulative infiltration data into an exceedance probability. This then can be used to pinpoint the time validity of Philip's two-term infiltration equation. As we can repeat this exercise for each posterior simulation, this gives rise to a probability distribution of t_{valid} for each soil type. This refined method carries forward any assumptions we may make with respect to the measurement errors of

the cumulative infiltration data, from definition of the likelihood function, to the posterior samples of the DREAM$_{(ZS)}$ algorithm, the marginal distribution of c_β, the chi-squared test statistic, and resulting time validities. Indeed, this refined method address more explicitly the uncertainty inherent in our estimates of t_{valid}.

We would be remiss not to comment on the use of real-world infiltration data. In our preliminary investigations presented herein, we purposely used synthetic infiltration data so that we can benchmark our sorptivity and saturated hydraulic conductivity estimates. Nothing prevents us from using either of the two methods to measured infiltration data. As Parlange's infiltration equation does not suffer a limited time validity, we can always use Step 1 of our methodology to infer the posterior parameter distribution of S, K_s, and β. Then, in Step 2, we can iterate over the measurements to determine the time validity of Philip's infiltration model and associated value of the multiplicative coefficient, c. Alternatively, one can use the refined approach describe above as replacement of Step 2, and turn the sampled β values into a marginal distribution of c values, followed by computation of the exceedance probabilities of the measured infiltration data. This ultimately provides a distribution of time validities for each measured infiltration dataset. Indeed, experiments carried out on measured data from the SWIG database confirm our main conclusions. However, the inferred time validities are less subtle, as the measured infiltration data generally exhibit a much poorer temporal resolution.

We like to comment last on the practical usefulness of our methodology. If the interest is only in the hydraulic properties

of the soil, then Step 1 of our methodology will suffice. The MATLAB code of Appendix A coupled with the DREAM$_{(ZS)}$ algorithm realizes the full potential of Parlange's infiltration equation for inverse estimation of soil hydraulic properties and will help rectify the abundant use by practitioners of more convenient analytical infiltration functions that suffer physical underpinning and/or a limited time validity. The posterior distribution of the Parlange parameters, S, K_s, and β is a witness of data quality and quantity. With few or poor infiltration measurements at early times, for example, the soil sorptivity will suffer and exhibit a relatively large posterior uncertainty. Short experiments, on the contrary, will complicate the inference of β as its impact on the simulated $I(t)$ relationship is negligible at early times of infiltration. This is easy to verify from the sensitivity matrix of Parlange's infiltration equation and promotes a flat posterior marginal distribution of β. The posterior uncertainty of S, K_s, and β can be propagated forward to quantify prediction intervals. What is more, if we adopt the $c(\beta)$ relationship of Equation 19, then Step 1 yields a marginal posterior distribution of coefficient c as well. The trivariate distribution of S, K_s, and c can enter Philip's two-term infiltration equation. The second step of our methodology serves a perhaps more academic purpose. Nevertheless, knowledge of the coefficient c and time validity, t_{valid}, of Philip's two-term expression is of utmost importance in the practical application of this infiltration equation.

6 | SUMMARY AND CONCLUSIONS

The two-term infiltration equation, $I(t) = S\sqrt{t} + cK_s t$, of Philip (1957) is widely used to infer the soil sorptivity, S, and saturated hydraulic conductivity, K_s, from a n-record of measured cumulative infiltration data, $\{\tilde{t}_i, \tilde{I}_i\}_{i=1}^n$. This infiltration equation is easy to use, supported by detailed mathematical–physical analysis, and the optimum values of S and K_s can be obtained from linear least squares via a closed-form expression. Despite this progress made, Philip's two-term infiltration function has a limited time validity, t_{valid}, and consequently, cumulative infiltration data, $\tilde{I}(\tilde{t})$, beyond $t = t_{valid}$, will corrupt the least squares estimates of S and K_s.

The contributions of this paper were twofold. First, we introduced a method that can successfully infer the sorptivity, S, saturated hydraulic conductivity, K_s, dimensionless coefficient, c, and time validity, t_{valid}, of Philip's two-term infiltration equation.

As prerequisite of this methodology, the second contribution of this work is a robust, exact and efficient numerical solution of Parlange's implicit infiltration equation. The proposed methodology was tested on 12 USDA soil types using HYDRUS-1D simulated infiltration data. Results demonstrated an excellent match between the inferred values of S and K_s and their "true" values with estimates of c and t_{valid}

that correlate well with soil texture and corroborate linearity of the $c(\beta)$ relationship for infiltration times up to t_{valid}. Additional experiments carried out on measured infiltration data from the SWIG database of Rahmati, Weihermüller, Vanderborght, et al. (2018) and Rahmati, Weihermüller, and Vereecken (2018) confirmed our main findings.

In the penultimate section of this paper, we described a modification to Step 2 of our method which takes advantage of the $c(\beta)$ relationship to determine the posterior parameter distribution of Philip's two-term infiltration equation. Its time validity can then be inferred using a χ^2 test of the cumulative infiltration residuals of each posterior simulation. This approach propagates forward assumptions made about the measurement error of the infiltration data to a marginal distribution of time validities for each soil.

CONFLICT OF INTEREST
The authors declare no conflict of interest.

DATA AND SOFTWARE AVAILABILITY
The data and software are available upon request from the corresponding author (jasper@uci.edu) and can be downloaded at the following URL: https://www.dropbox.com/sh/xpgpe8mu9pquyva/AAASIRsnJU7Q2FO6RAF_MD4
Ta?dl=0.

ORCID
Mehdi Rahmati https://orcid.org/0000-0001-5547-6442
Harry Vereecken https://orcid.org/0000-0002-8051-8517
Jasper A. Vrugt https://orcid.org/0000-0003-2599-1165

REFERENCES
Assouline, S. (2013). Infiltration into soils: Conceptual approaches and solutions. *Water Resources Research*, *49*, 1755–1772. https://doi.org/10.1002/wrcr.20155

Barry, D. A., Parlange, J.-Y., Haverkamp, R., & Ross, P. J. (1995). Infiltration under ponded conditions: 4. An explicit predictive infiltration

formula. *Soil Science*, *160*, 8–17. https://doi.org/10.1097/00010694-199507000-00002

Basha, H. A. (1999). Multidimensional linearized nonsteady infiltration with prescribed boundary conditions at the soil surface. *Water Resources Research*, *35*, 75–93. https://doi.org/10.1029/1998WR900015

Basha, H. A. (2000). Multidimensional quasi-linear steady infiltration toward a shallow water table. *Water Resources Research*, *36*(7), 1697–1705. https://doi.org/10.1029/2000WR900064

Basha, H. A. (2002). Burger's equation: A general nonlinear solution of infiltration and redistribution. *Water Resources Research*, *38*(11). https://doi.org/10.1029/2001WR000954

Braester, C. (1973). Moisture variation at the soil surface and the advance of the wetting front during infiltration at constant flux. *Water Resources Research*, *9*(11), 687–694. https://doi.org/10.1029/WR009i003p00687

Brooks, S. P., & Gelman, A. (1998). General methods for monitoring convergence of iterative simulations. *Journal of Computational and Graphical Statistics*, *7*, 434–455.

Brutsaert, W. (1977). Vertical infiltration in dry soil. *Water Resources Research*, *13*, 363–368. https://doi.org/10.1029/WR013i002p00363

Carsel, R. F., & Parrish, R. S. (1988). Developing joint probability distributions of soil water retention characteristics. *Water Resources Research*, *24*(5), 755–769. https://doi.org/10.1029/WR024i005p00755

Chen, C., & Gallipoli, D. (2004). Steady infiltration from buried point source into heterogeneous cross-anisotropic unsaturated soil. *International Journal for Numerical and Analytical Methods in Geomechanics*, *28*, 1033–1055. https://doi.org/10.1002/nag.370

Chen, X., Luo, Z., & Zhou, S. (2014). Influences of soil hydraulic and mechanical parameters on land subsidence and ground fissures caused by groundwater exploitation. *Journal of Hydrodynamics*, *26*(1), 155–164. https://doi.org/10.1016/S1001-6058(14)60018-4

Collis-George, N. (1977). Infiltration equations for simple soil systems. *Water Resources Research*, *13*, 395–403. https://doi.org/10.1029/WR013i002p00395

Dohnal, M., Dusek, J., & Vogel, T. (2010). Improving hydraulic conductivity estimates from minidisk infiltrometer measurements for soils with wide pore-size distributions. *Soil Science Society of America Journal*, *74*, 804–811. https://doi.org/10.2136/sssaj2009.0099

Fernández-Gálvez, J., Pollacco, J. A. P., Lassabatere, L., Angulo-Jaramillo, R., & Carrick, S. (2019). A general Beerkan estimation of soil transfer parameters method predicting hydraulic parameters of any unimodal water retention and hydraulic conductivity curves: Application to the Kosugi soil hydraulic model without using particle size distribution data. *Advances in Water Resources*, *129*, 118–130. https://doi.org/10.1016/j.advwatres.2019.05.005

Fisher, R. A. (1934). *Statistical methods for research workers*. Oliver & Boyd.

Fuentes, C., Haverkamp, R., & Parlange, J.-Y. (1992). Parameter constraints on closed-form soil water relationships. *Journal of Hydrology*, *134*, 117–142. https://doi.org/10.1016/0022-1694(92)90032-Q

Green, W. H., & Ampt, G. A. (1911). Studies on soil physics. *The Journal of Agricultural Science*, *4*(1), 1–24. https://doi.org/10.1017/S0021859600001441

Grigorjev, V. Y., & Iritz, L. (1991). Dynamic simulation model of vertical infiltration of water in soil. *Hydrological Sciences Journal*, *36*(2), 171–179. https://doi.org/10.1080/02626669109492497

Haverkamp, R., Parlange, J.-Y., Starr, J. L., Schmitz, G., & Fuentes, C. (1990). Infiltration under ponded conditions: 3. A predictive equation based on physical parameters. *Soil Science*, *149*, 292–300. https://doi.org/10.1097/00010694-199005000-00006

Haverkamp, R., Ross, P. J., Smettem, K. R. J., & Parlange, J. - Y. (1994). Three-dimensional analysis of infiltration from the disc infiltrometer: 2. Physically based infiltration equation. *Water Resources Research*, *30*(11), 2931–2935. https://doi.org/10.1029/94WR01788

Hellin, J., & Schrader, K. (2003). The case against direct incentives and the search for alternative approaches to better land management in Central America. *Agriculture, Ecosystems & Environment*, *99*(1), 61–81.

Holtan, H. N. (1961). *A concept for infiltration estimates in watershed engineering*. USDA-ARS.

Horton, R. E. (1933). The role of infiltration in the hydrologic cycle. *Eos, Transactions American Geophysical Union*, *14*(1), 446–460. https://doi.org/10.1029/TR014i001p00446

Horton, R. E. (1941). An approach toward a physical interpretation of infiltration-capacity. *Soil Science Society of America Journal*, *5*(100), 399–417. https://doi.org/10.2136/sssaj1941.036159950005000C0075x

Huggins, L. F., & Monke, E. J. (1966). *The mathematical simulation of the hydrology of small watersheds* (Indiana Water Resources Research Center Technical Reports 8-1-1966). Purdue University.

Hunt, A. G., Holtzman, R., & Ghanbarian, B. (2017). A percolation-based approach to scaling infiltration and evapotranspiration. *Water*, *9*(2). https://doi.org/10.3390/w9020104

Kostiakov, A. N. (1932). On the dynamics of the coefficient of water percolation in soils and the necessity of studying it from the dynamic point of view for the purposes of amelioration. In O. Fauser (Ed.), *Transactions of Sixth Committee International Society of Soil Science* (pp. 7–21). International Society of Soil Science.

Laloy, E., Linde, N., Jacques, D., & Vrugt, J. A. (2015). Probabilistic inference of multi-Gaussian fields from indirect hydrological data using circulant embedding and dimensionality reduction. *Water Resources Research*, *51*, 4224–4243. https://doi.org/10.1002/2014WR016395

Lassabatere, L., Angulo-Jaramillo, R., Soria-Ugalde, J. M., Šimůnek, J., & Haverkamp, R. (2009). Numerical evaluation of a set of analytical infiltration equations. *Water Resources Research*, *45*(12). https://doi.org/10.1029/2009WR007941

Latorre, B., Moret-Fernández, D., Lassabatere, L., Rahmati, M., López, M. V., Angulo-Jaramillo, R., Sorando, R., Comín, F., & Jiménez, J. J. (2018). Influence of the beta parameter of the Haverkamp model on the transient soil water infiltration curve. *Journal of Hydrology*, *564*, 222–229. https://doi.org/10.1016/j.jhydrol.2018.07.006

Latorre, B., Peña, C., Lassabatere, L., Angulo-Jaramillo, R., & Moret-Fernández, D. (2015). Estimate of soil hydraulic properties from disc infiltrometer three-dimensional infiltration curve. numerical analysis and field application. *Journal of Hydrology*, *527*, 1–12. https://doi.org/10.1016/j.jhydrol.2015.04.015

Linde, N., & Vrugt, J. A. (2013). Distributed soil moisture from cross-hole ground-penetrating radar travel times using stochastic inversion. *Vadose Zone Journal*, *12*(1), 1–16. https://doi.org/10.2136/vzj2012.0101

Liu, H., Lei, T. W., Zhao, J., Yuan, C. P., Fan, Y. T., & Qu, L. Q. (2011). Effects of rainfall intensity and antecedent soil water content on soil infiltrability under rainfall conditions using the run off-on-

out method. *Journal of Hydrology*, *396*(1), 24–32. https://doi.org/10.1016/j.jhydrol.2010.10.028

Mein, R. G., & Larson, C. L. (1971). *Modeling the infiltration component of the rainfall-runoff process*. Water Resources Research Center, University of Minnesota.

Mein, R. G., & Larson, C. L. (1973). Modeling infiltration during a steady rain. *Water Resources Research*, *9*(2), 384–394. https://doi.org/10.1029/WR009i002p00384

Moret-Fernández, D., Latorre, B., & Angulo-Martínez, M. (2017). Comparison of different methods to estimate the soil sorptivity from an upward infiltration curve. *Catena*, *155*, 86–92. https://doi.org/10.1016/j.catena.2017.03.009

Moret-Fernández, D., Latorre, B., López, M. V., Pueyo, Y., Lassabatere, L., Angulo-Jaramilo, R., Rahmati, M., Tormo, J., & Nicolau, J. M. (2020). Three- and four-term approximate expansions of the Haverkamp formulation to estimate soil hydraulic properties from disc infiltrometer measurements. *Hydrological Processes*, *34*(26), 5543–5556. https://doi.org/10.1002/hyp.13966

Mualem, Y. (1976). A new model for predicting the hydraulic conductivity of unsaturated porous media. *Water Resources Research*, *12*(3), 513–522. https://doi.org/10.1029/WR012i003p00513

Parlange, J.-Y., Haverkamp, R., & Touma, J. (1985). Infiltration under ponded conditions: 1. optimal analytical solution and comparison with experimental observations. *Soil Science*, *139*, 305–311. https://doi.org/10.1097/00010694-198504000-00003

Parlange, J.-Y., Lisle, I., Braddock, R. D., & Smith, R. E. (1982). The three-parameter infiltration equation. *Soil Science*, *133*(6), 337–341. https://doi.org/10.1097/00010694-198206000-00001

Philip, J. R. (1957). The theory of infiltration: 1. The infiltration equation and its solution. *Soil Science*, *83*(5), 345–358. https://doi.org/10.1097/00010694-195705000-00002

Philip, J. R. (1969a). Moisture equilibrium in the vertical in swelling soils. I. Basic theory. *Soil Research*, *7*(2), 99–120. https://doi.org/10.1071/SR9690099

Philip, J. R. (1969b). Theory of infiltration. *Advances in Hydroscience*, *5*, 215–296. https://doi.org/10.1016/B978-1-4831-9936-8.50010-6

Popper, K. (1992). *The logic of scientific discovery*. Routledge.

Qin, H., Vrugt, J. A., Xie, X., & Zhou, Y. (2018). Improved characterization of underground structure defects from two-stage Bayesian inversion using crosshole GPR data. *Automation in Construction*, *95*, 233–244. https://doi.org/10.1016/j.autcon.2018.08.014

Rahmati, M., Latorre, B., Lassabatere, L., Angulo-Jaramillo, R., & Moret-Fernández, D. (2019). The relevance of Philip theory to Haverkamp quasi-exact implicit analytical formulation and its uses to predict soil hydraulic properties. *Journal of Hydrology*, *570*, 816–826. https://doi.org/10.1016/j.jhydrol.2019.01.038

Rahmati, M., Vanderborght, J., Šimůnek, J., Vrugt, J. A., Moret-Fernández, D., Latorre, B., Lassabatere, L., & Vereecken, H. (2020). Soil hydraulic properties estimation from one-dimensional infiltration experiments using characteristic time concept. *Vadose Zone Journal*, *19*, 1–22. https://doi.org/10.1002/vzj2.20068

Rahmati, M., Weihermüller, L., Vanderborght, J., Pachepsky, Y. A., Mao, L., Sadeghi, S. H., Moosavi, N., Kheirfam, H., Montzka, C., Van Looy, K., Toth, B., Hazbavi, Z., Al Yamani, W., Albalasmeh, A. A., Alghzawi, M. Z., Angulo-Jaramillo, R., Antonino, A. C. D., Arampatzis, G., Armindo, R. A., . . . , & Vereecken, H. (2018). Development and analysis of the Soil Water Infiltration Global database. *Earth System Science Data*, *10*(3), 1237–1263. https://doi.org/10.5194/essd-10-1237-2018

Rahmati, M., Weihermüller, L., & Vereecken, H. (2018). Soil Water Infiltration Global (SWIG) database [Supplement to: Rahmati, M et al. (2018): Development and analysis of Soil Water Infiltration Global database]. *Earth System Science Data*. https://doi.org/10.1594/PANGAEA.885492

Salvucci, G., & Entekhabi, D. (1994). Explicit expressions for Green-Ampt (delta function diffusivity) infiltration rate and cumulative storage. *Water Resources Research*, *30*, 2661–2663. https://doi.org/10.1029/94WR01494

Schaap, M. G., & van Genuchten, M. Th. (2006). A modified Mualem-van Genuchten formulation for improved description of the hydraulic conductivity near saturation. *Vadose Zone Journal*, *5*(1), 27–34. https://doi.org/10.2136/vzj2005.0005

Schoups, G., Hopmans, J. W., Young, C. A., Vrugt, J. A., Wallender, W. W., Tanji, K. K., & Panday, S. (2005). Sustainability of irrigated agriculture in the San Joaquin Valley, California. *Proceedings of the National Academy of Sciences*, *102*(43), 15352–15356. https://doi.org/10.1073/pnas.0507723102

Šimůnek, J., van Genuchten, M. Th., & Sejna, M. (2008). Development and applications of the HYDRUS and STANMOD software packages and related codes. *Vadose Zone Journal*, *7*(2), 587–600. https://doi.org/10.2136/vzj2007.0077

Šimůnek, J., van Genuchten, M. Th., & Sejna, M. (2016). Recent developments and applications of the HYDRUS computer software packages. *Vadose Zone Journal*, *15*(7). https://doi.org/10.2136/vzj2016.04.0033

Singh, V., & Yu, F. X. (1990). Derivation of infiltration equation using systems approach. *Journal of Irrigation and Drainage Engineering*, *116*, 837–858. https://doi.org/10.1061/(ASCE)0733-9437(1990)116:6(837)

Smith, R. E. (1972). The infiltration envelope: Results from a theoretical infiltrometer. *Journal of Hydrology*, *17*(1), 1–22. https://doi.org/10.1016/0022-1694(72)90063-7

Smith, R. E., & Parlange, J.-Y. (1978). A parameter-efficient hydrologic infiltration model. *Water Resources Research*, *14*, 533–538. https://doi.org/10.1029/WR014i003p00533

Stroosnijder, L. (1976). Cumulative infiltration and infiltration rate in homogeneous soils. *Agricultural Research*, *847*, 69–99.

Valiantzas, J. D. (2010). New linearized two-parameter infiltration equation for direct determination of conductivity and sorptivity. *Journal of Hydrology*, *384*(1–2), 1–13. https://doi.org/10.1016/j.jhydrol.2009.12.049

van Genuchten, M. Th. (1980). A closed-form equation for predicting the hydraulic conductivity of unsaturated soils. *Soil Science Society of America Journal*, *44*(5), 892–898. https://doi.org/10.2136/sssaj1980.03615995004400050002x

Vogel, T., & Cislerova, M. (1988). On the reliability of unsaturated hydraulic conductivity calculated from the moisture retention curve. *Transport in Porous Media*, *3*(1), 1–15. https://doi.org/10.1007/BF00222683

Vogel, T., van Genuchten, M. Th., & Cislerova, M. (2000). Effect of the shape of the soil hydraulic functions near saturation on variably-saturated ow predictions. *Advances in Water Resources*, *24*(2), 133–144. https://doi.org/10.1016/S0309-1708(00)00037-3

Volpi, E., Schoups, G., & Fermani, G. (2017). Sworn testimony of the model evidence: Gaussian mixture importance (GAME) sampling. *Water Resources Research*, *53*, 6133–6158. https://doi.org/10.1002/2016WR020167

Vrugt, J. A. (2016). Markov chain Monte Carlo simulation using the DREAM software package: Theory, concepts, and MATLAB implementation. *Environmental Modeling & Software*, 75, 273–316.

Vrugt, J. A., & Massoud, E. C. (2019). Uncertainty quantification of complex system models: Bayesian analysis. In Q. Duan, F. Pappenberger, A. Wood, H. L. Cloke, & J. C. Schaake (Eds.), *Handbook of hydrometeorological ensemble forecasting* (pp. 563–636). Springer.

Vrugt, J. A., ter Braak, C. J. F., Clark, M. P., Hyman, J. M., & Robinson, B. A. (2008). Treatment of input uncertainty in hydrologic modeling: Doing hydrology backward with Markov chain Monte Carlo simulation. *Water Resources Research*, 44, W00B09. https://doi.org/10.1029/2007WR006720

Vrugt, J. A., ter Braak, C. J. F., Diks, C., Robinson, B. A., Hyman, J. M., & Higdon, D. (2009). Accelerating Markov chain Monte Carlo simulation by differential evolution with self-adaptive randomized subspace sampling. *International Journal of Nonlinear Sciences & Numerical Simulation*, 10(3), 273–290.

Zhang, J., Vrugt, J. A., Shi, X., Lin, G., Wu, L., & Zeng, L. (2020). Improving simulation efficiency of MCMC for inverse modeling of hydrologic systems with a Kalman-inspired proposal distribution. *Water Resources Research*, 56, 1–24. https://doi.org/10.1029/2019WR025474

Zhu, J., & Mohanty, B. P. (2002). Analytical solutions for steady-state vertical infiltration. *Water Resources Research*, 38(8). https://doi.org/10.1029/2001WR000398

SUPPORTING INFORMATION

Additional supporting information may be found in the online version of the article at the publisher's website.

APPENDIX A

This appendix presents the implementation of our numerical solution of Parlange's infiltration equation in MATLAB. Based on the 4×1 vector, η, with values of the sorptivity, S (cm h$^{-1/2}$), saturated hydraulic conductivity, K_s (cm h^{-1}), unitless coefficient, β, and initial hydraulic conductivity, K_i, and the $n \times 1$ vector, $\mathbf{t}$, with discretized values of time in dimension of hour, the MATLAB function Parlange returns the cumulative infiltration, I, and infiltration rate, i (in units of cm and cm h^{-1}, respectively), and an exit flag, flag, which

reports the corresponding exit condition of the secant method (see Figure A1).

The user may specify two additional input arguments, tolfun and maxiter, which equal the desired tolerance on the function value at the final root and the maximum number of iterations of the secant method, respectively. These last two input arguments are optional. If omitted in the Parlange function call, tolfun and maxiter will be assigned default values of 10^{-12} and 20, respectively. Built-in functions are highlighted with a underlining.

The Parlange function calls the function secant, which solves for the zero-point of Parlange's residual function (S1.7) at each time, t (see Figure A2).

The secant function has three required input arguments—namely, fun, an anonymous function handle of Parlange's residual function, and Ii1 and Ii2, which define the initial search bracket, $[I_{(0)}, I_{(1)}]$, of the root of $r(I,t)$. The secant method may not always be used in each iteration of the Parlange function. For the secant method to work in practice, the residual function, $r(I,t)$, at the upper bound, $I_{(1)}$, of the initial search bracket, $[I_{(0)}, I_{(1)}]$, cannot be infinity, nor be smaller than 10^{-10}, hence, $10^{-10} < r[I_{(1)}, t] < \infty$. If $r[I_{(1)}, t] \leq 10^{-10}$, then our upper bound, $I_{(1)}$, is very close to the actual root. Hence, we can use, $I_{(1)}$, as our solution of $I(t)$. A value of $r[I_{(1)}, t]$ equal to infinity is a numerical artifact. The term $\exp[2\beta\xi(I - K_i t)]$ in Parlange's residual function (S1.7) may return infinity for certain (often implausible) combinations of S, K_s, and β, as the exponential function grows larger than its limit on a 64-bit computer. This is called numerical overflow and is typically restricted to saturated conditions. At this time, the soil has reached a constant infiltration rate and, thus, we can make use of the identity, $I_{(k)} = I_{(k-1)} + [t_{(k)} - t_{(k-1)}]K_s$, to solve for the remaining part of the cumulative infiltration curve.

The Parlange function has been evaluated numerous times for $K_i = 0$ and $0 \leq t \leq 240$ using Monte Carlo simulation with $S \in (0, 10]$ (cm h$^{-1/2}$), $K_s \in (0, 50]$ (cm h^{-1}), and $\beta \in (0, 2)$. The resulting $I(t)$ curves were compared against a direction solution of $t(I)$ derived with $K_i = 0$ using a swap of the independent and dependent variables. This comparison has shown that the simulated cumulative infiltration curves of the Parlange function are almost exact with a negligible numerical error. In 1,000 separate trials, the code would terminate prematurely a handful of times in response to numerical underflow of the exponential function. This can be avoided by setting a lower limit of, say, 10^{-4} on the values of β. Altogether, our experiments have shown that the Parlange function is robust, efficient, and exact.

```matlab
function [I,i,flag] = Parlange(eta,t,tolfun,maxiter)
%% %%%%%%%%%%%%%%%%%%%%%%%%%%%%%%%%%%%%%%%%%%%%%%%%%%%%%%%%%%%%%%%%%%%%%%% %%
%% This function solves for the I(t) relationship of the three-parameter infiltration %%
%% equation of Parlange (1982) using the secant method                 %%
%%  SYNOPSIS: I = Parlange(eta,t)                                      %%
%%            I = Parlange(eta,t,tolfun)                               %%
%%            I = Parlange(eta,t,tolfun,maxiter)                       %%
%% where                                                              %%
%%  eta      [in]       4x1 vector with S (cm/h^0.5), Ks (cm/h), beta (-), Ki (cm/h)  %%
%%  t        [in]       nx1 vector with time, t, in hours (h)          %%
%%  tolfun   [opt. in]  tolerance on function value at root      (default: 1e-12)  %%
%%  maxiter  [opt. in]  maximum number of secant iterations      (default: 20)    %%
%%  I        [out]      cumulative infiltration, I (cm), as function of time, t (h)  %%
%%  i        [out]      infiltration rate, i (cm/h), as function of time, t (h)      %%
%%  flag     [out]      exit: [1] fine [-2] inf. root [-3] inf. func. [-4] imag. func. %%
%% %%%%%%%%%%%%%%%%%%%%%%%%%%%%%%%%%%%%%%%%%%%%%%%%%%%%%%%%%%%%%%%%%%%%%%% %%
if nargin < 4, maxiter = 20; end
if nargin < 3, tolfun = 1e-12; end
if numel(eta) == 3, eta(4) = 0; end
%% Initialization part: problem setup
S = eta(1); Ks = eta(2); B = eta(3); Ki = eta(4);    % Unpack parameter values
dK = Ks - Ki; xi = dK/S^2; t = t(:); n = numel(t);   % Compute dK and xi, # elements t
I = nan(n,1); I(1) = 0;                              % Initial cum. inf.
if dK <= 0, return; end                              % If dK <= 0, return I = nan(n,1)
if t(1) == 0                                         % Check if first time is zero
    j = 2; dt = [ 0; diff(t) ];                      %   Yes: start t(2), define dt
else                                                 % otherwise
    j = 1; dt = [ t(1) ; diff(t) ];                  %   No: start t(1), define dt
end                                                  % End statement
r = @(I,t) dK*(1-B)*t + Ki*t - I + ...               % Residual function
    1/(2*xi)*log(1/B*exp(2*B*xi*(I-Ki*t))) + (B-1)/B);
Ii0 = 0; t0 = 0;                                     % Lower end search bracket
%% Dynamic part: compute infiltration at each time
for k = j:n                                          % For loop
    Ii1 = Ii0 + S*(sqrt(t(k))-sqrt(t0)) + dt(k)*Ks;  % Upper end search bracket
    if abs(r(Ii1,t(k)))>tolfun && abs(r(Ii1,t(k)))<inf  % Conditions secant method
        [I(k),flag] = secant(@(y) r(y,t(k)),...              % I(k) from secant method
            Ii0,Ii1,tolfun,maxiter);
        if flag ~= 1                                        % Check flag
            warning('Terminated prematurely'); return         % Terminate function
        end                                                 % End statement
    else                                             % Otherwise
        I(k) = Ii0 + dt(k)*Ks; flag = 1;                 % I(k) from constant rate
        warning('Steady-state assumption');              % Print warning
    end                                              % End statement
    Ii0 = I(k); t0 = t(k);                           % Lower-end search bracket
end                                                  % End for loop
A = exp(2*B*xi*(I-Ki*t));                            % Compute alpha
i = (((1-B)*Ks+B*Ki)*(A+B-1)-A*B*Ki)./(A+B-A*B-1);  % Compute infiltration rate
```

F I G U R E A 1   MATLAB code of the Parlange function

```matlab
function [Ir,exitflag] = secant(r,Ii0,Ii1,tolfun,maxiter)
%% %%%%%%%%%%%%%%%%%%%%%%%%%%%%%%%%%%%%%%%%%%%%%%%%%%%%%%%%%%%%%%%%%%%%%%%% %%
%% The Secant method for root finding of infiltration equation of Haverkamp   %%
%%  SYNOPSIS: [Ir,exitflag] = secant(r,Ii0,Ii1)                              %%
%%            [Ir,exitflag] = secant(r,Ii0,Ii1,tolfun)                       %%
%%            [Ir,exitflag] = secant(r,Ii0,Ii1,tolfun,maxiter)               %%
%% where                                                                      %%
%%  r       [in] anonymous function handle of residual function Haverkamp     %%
%%  Ii0     [in] lower end initial search bracket (cumulative infiltration in cm) %%
%%  Ii1     [in] upper end initial search bracket (cumulative infiltration in cm) %%
%%  tolfun  [opt. in] tolerance on root function value (default: 1e-12)       %%
%%  maxiter [opt. in] maximum number of iterations (default: 20)             %%
%%  Ir      [out] cumulative infiltration (in cm) at specified time           %%
%%  exitflag [out] exit condition. Possible conditions are:                  %%
%%                   1: secant found a proper zero point (= root)             %%
%%                  -2: secant terminated with infinite root                  %%
%%                  -3: secant terminated with infinite function value at root %%
%%                  -4: secant terminated with imaginary function value at root %%
%% %%%%%%%%%%%%%%%%%%%%%%%%%%%%%%%%%%%%%%%%%%%%%%%%%%%%%%%%%%%%%%%%%%%%%%%% %%

%% Initialization part: problem setup
if nargin < 5, maxiter = 20; end              % Default value of maxiter?
if nargin < 4, tolfun = 1e-12; end            % Default value of tolfun?
k = 3;                                         % Set iteration counter
I(1) = Ii0; I(2) = Ii1;                        % [Ii0,Ii1] root bracket
I(3) = (I(1)*r(I(2))-I(2)*r(I(1))) ...         % Next guess of root
    / (r(I(2))-r(I(1)));

%% Dynamic part: secant method
while (abs(r(I(k))) > tolfun) && (k-2 < maxiter)   % While loop
    k = k + 1;                                       % Increment iteration
    I(k) = (I(k-2)*r(I(k-1))-I(k-1)*r(I(k-2))) ...   % New guess of root
        / (r(I(k-1))-r(I(k-2)));
end                                                % End of while loop

%% Postprocessing part: determine exit condition
Ir = I(k); fIr = r(Ir);                        % Root and function value
if ~isfinite(Ir)                               % Infinite value of root?
    exitflag = -2;                             % Yes: return -2
elseif ~isfinite(fIr)                          % Infinite function value root?
    exitflag = -3;                             % Yes: return -3
elseif ~isreal(fIr)                            % Imaginary function value root?
    exitflag = -4;                             % Yes: return -4
else                                           % All other cases
    exitflag = 1;                              % Return 1
end
```

FIGURE A2   MATLAB code of the secant method